

1 **Underappreciated contributions of biogenic volatile organic compounds from urban**  
2 **greening to ozone pollution: a high-resolution modeling study**

3  
4 Haofan Wang<sup>1,2,3,4</sup>, Yuejin Li<sup>1,2,3</sup>, Yiming Liu<sup>1,2,3\*</sup>, Xiao Lu<sup>1,2,3</sup>, Yang Zhang<sup>5</sup>, Qi Fan<sup>1,2,3\*</sup>, Chong Shen<sup>6</sup>,  
5 Senchao Lai<sup>7</sup>, Yan Zhou<sup>7</sup>Zhou<sup>8</sup>, Tao Zhang<sup>7</sup>Zhang<sup>8</sup>, Dingli Yue<sup>7</sup>Yue<sup>8</sup>

6  
7 <sup>1</sup>*School of Atmospheric Sciences, Sun Yat-sen University, and Southern Marine Science and Engineering Guangdong Laboratory  
8 (Zhuhai), Zhuhai, 519082, P. R. China*

9 <sup>2</sup>*Guangdong Provincial Field Observation and Research Station for Climate Environment and Air Quality Change in the Pearl  
10 River Estuary, Guangzhou, 510275, P. R. China*

11 <sup>3</sup>*Guangdong Province Key Laboratory for Climate Change and Natural Disaster Studies, Sun Yat-sen University, P. R. China*

12 <sup>4</sup>*Centre for Atmospheric Science, Department of Earth and Environmental Sciences, The University of Manchester, Manchester,  
13 United Kingdom*

14 <sup>5</sup>*College of Resources and Environment, Chengdu University of Information Technology, Chengdu, Sichuan, China*

15 <sup>6</sup>*Guangzhou Climate and Agrometeorology Center, Guangzhou 511430, China*

16 <sup>7</sup>National<sup>7</sup>The Key Lab of Pollution Control and Ecosystem Restoration in Industry Clusters, Ministry of Education, School of  
17 Environment and Energy, South China University of Technology, Guangzhou 510006, China

18 <sup>8</sup>National<sup>8</sup>Key Laboratory for Regional Air Quality Monitoring of Environmental Protection/Guangdong Ecological Environment  
19 Monitoring Center, Guangzhou 510308, P. R. China

20  
21 *Correspondence to: Yiming Liu ([liuym88@mail.sysu.edu.cn](mailto:liuym88@mail.sysu.edu.cn)), Qi Fan ([eesfq@mail.sysu.edu.cn](mailto:eesfq@mail.sysu.edu.cn))*

23 **Abstract**

24 Urban Green Spaces (UGS), such as parks, and gardens, are widely promoted as a strategy for improving the  
25 urban atmosphere and environmental health. However, this study reveals that it can exacerbate urban ozone  
26 ( $O_3$ ) levels under certain conditions, as demonstrated by a September 2017 study in Guangzhou, China.  
27 Utilizing the Weather Research and Forecasting Model with the Model of Emissions of Gases and Aerosols  
28 from Nature (WRF-MEGAN) and the Community Multiscale Air Quality (CMAQ) model with a high  
29 horizontal resolution (1 km), we assessed the impact of UGS-related biogenic volatile organic compound  
30 (BVOC) emissions on urban  $O_3$ . Our findings indicate that the UGS-BVOC emissions in Guangzhou  
31 amounted to 666 Gg (~90 Mg/km<sup>2</sup>), with isoprene (ISOP) and monoterpene (TERP) contributing remarkably  
32 to the total UGS-BVOC emissions. In comparison to anthropogenic VOC (AVOC) and BVOC emissions,  
33 UGS-BVOC emissions account for approximately 33.45% in the city center region. Incorporating UGS-  
34 BVOC emissions into the model significantly reduces the underestimation of ISOP levels compared to  
35 observations. The study shows improvements in simulation mean biases for  $NO_2$ , from 3.27 to 2.81 ppb, and  
36 for MDA8  $O_3$ , from -3.6263 to -0.75 ppb in the city center region. UGS-BVOC and UGS-LUCC (land use  
37 cover changes) integration in the air quality model notably enhances surface monthly mean  $O_3$  predictions by  
38 1.7-3.7 ppb (+3.8-8.5%) and contributes up to 8.9 ppb (+10.0%) to MDA8  $O_3$  during  $O_3$  pollution episodes.  
39 Additionally, UGS-BVOC emissions alone increase the monthly mean  $O_3$  levels by 1.0-1.4 ppb (+2.3-3.2%)  
40 in urban areas and contribute up to 2.9 ppb (+3.3%) to MDA8  $O_3$  levels during  $O_3$  pollution episodes. These  
41 impacts can extend to surrounding suburban and rural areas through regional transport, highlighting the  
42 importance of accurately accounting for UGS-BVOC emissions to better understand and manage their impact  
43 on regional air quality.

44 **Keywords**

45 Urban green space; BVOC; Ozone; Land use cover; CMAQ; MEGAN

46

47 **1. Introduction**

48 Exposure to air pollution now accounts for more fatalities than malaria, tuberculosis, and HIV/AIDS combined

49 (Lelieveld et al., 2020). As a result, the World Health Organization has declared air pollution the most  
50 significant environmental threat to human health (WHO, 2021). Notably, over 70% global health burden of  
51 air pollution stems from human-made emissions, leading to a policy focus predominantly on reducing these  
52 emissions (Chowdhury et al., 2022; Lelieveld et al., 2019). Despite proactive measures to curb anthropogenic  
53 emissions, the incidence of ozone episodes is escalating alongside rapid urbanization (Lu et al., 2020; Yim et  
54 al., 2019). Numerous studies have investigated the effects of land use cover changes (LUCC) on air quality  
55 during urbanization using numerical models and the majority of these studies conclude that urbanization  
56 exacerbates air pollution (Qiu et al., 2023; Wang et al., 2022). However, such studies that depend on numerical  
57 models usually face the coarse-resolution land use cover data limitation (Ma et al., 2022, 2019), which leads  
58 these studies to frequently overlook a passive abatement approach distinct from reducing anthropogenic  
59 sources—namely, the cultivation of urban green spaces (UGS) (Cohen et al., 2017).

60  
61 The widely accepted notion that UGS can enhance air quality is substantiated by various strands of literature,  
62 including public health (Burnett et al., 2018), urban planning (Solomon, 2007), and ecosystem services  
63 (Lohmann et al., 2010). This concept is not only prevalent in scholarly circles but also gains traction in popular  
64 media and is echoed in international standards and policy frameworks. For instance, the United Nations  
65 System of Environmental-Economic Accounting advocates for vegetation as a nature-based approach to  
66 mitigate air pollution (Le Page et al., 2015). Vegetation primarily contributes to air pollution reduction through  
67 two mechanisms: deposition and dispersion (Shindell et al., 2012). Deposition involves the absorption of air  
68 pollutants onto vegetative surfaces, while dispersion refers to the reduction of air pollutant concentrations  
69 through aerodynamic effects caused by vegetation (Tiwari and Kumar, 2020; N. Wang et al., 2019a). Notably,  
70 Ramanathan et al. (2001) reported that dispersion effects are significantly more impactful than deposition,  
71 exceeding it by an order of magnitude via a radiative forcing modeling method.

72  
73 However, the efficacy of dispersion effects resulting from UGS-LUCC in reducing air pollution is not  
74 straightforward. These effects can, under certain conditions, even increase local air pollution concentrations.  
75 These conditions are influenced by several factors, such as the specific structure of the UGS vegetation  
76 properties (e.g., height, leaf density), the site context (e.g., street canyon geometry, proximity to emission  
77 sources), and prevailing meteorological conditions (e.g., wind speed and direction) (Jin et al., 2017; Tomson  
78 et al., 2021; Yang et al., 2020). For example, dense tree canopies might impede ventilation in urban street  
79 canyons, while porous vegetation barriers in open-road settings could potentially intensify roadside air

80 pollution concentrations (Chen et al., 2021; Jin et al., 2014). Furthermore, Seinfeld et al., (1998) underscores  
81 the complexity of these interactions, and demonstrated that vegetation could exert nonlinear effects on  
82 meteorological processes. These effects are particularly evident in their impact on the Planetary Boundary  
83 Layer Height (PBLH) and the turbulent transport and advection of pollutants, which in turn influence  
84 dispersion conditions.

85  
86 UGS also have a complex role in air quality due to their production of biogenic volatile organic compounds  
87 (BVOCs). For instance, in cities like Los Angeles, the UGS-BVOC emissions contribute to a quarter of the  
88 secondary organic aerosol formation on hot days (Schlaerth et al., 2023). While Guenther et al., (2012) noted  
89 that the majority of BVOC emissions are from natural land cover, Ma et al., (2022) indicates that in  
90 metropolitan areas, the UGS-BVOC emissions can be significantly higher, ranging from 1 to 30 times those  
91 from natural land use cover. This evidence suggests a dual nature of UGS vegetation in urban environments:  
92 it can mitigate air pollution under certain conditions, but conversely, there is substantial experimental and  
93 modeling evidence showing it can exacerbate pollution under different circumstances (Allen and Ingram, 2002;  
94 Burnett et al., 2018; Cohen et al., 2017). Moreover, metropolitan areas often encounter VOC-limited  
95 conditions, or NO<sub>x</sub>-saturation, where even minimal BVOC emissions can lead to notable O<sub>3</sub> production (P.  
96 Wang et al., 2019). Additionally, urban areas typically experience higher temperatures than their surrounding  
97 natural landscapes due to the urban heat island effect (Masson-Delmotte et al., 2021). This increase in  
98 temperature is likely to further amplify the UGS-BVOC emissions (Zhou et al., 2015), influencing O<sub>3</sub>  
99 concentrations significantly. This interaction might explain why many regional numerical models  
100 underestimate urban surface ozone levels, as they often lack high-resolution land use cover data necessary to  
101 accurately estimate the UGS-BVOC emissions (Qiu et al., 2023; Wang et al., 2021; Wu et al., 2020).

102  
103 Currently, there is a growing research interest in characterizing the air quality impacts of UGS. While  
104 Arghavani et al., (2019) investigated the effects of UGS on gaseous air pollutants in Tehran using the WRF-  
105 Chem model, their focus was on the impact of meteorological changes on O<sub>3</sub> resulting from UGS (i.e., UGS-  
106 LUCC effects), rather than the UGS-BVOC emissions effects on O<sub>3</sub>. In contrast, Schlaerth et al., (2023a)  
107 addressed the influence of the UGS-BVOC emissions on O<sub>3</sub> in Los Angeles and their findings indicate that  
108 the UGS-BVOC emissions may increase O<sub>3</sub> by 0.95 ppb during the daytime and decrease it by 0.41 ppb at  
109 night. Despite Schlaerth et al., (2023a) illustrating the significance of the UGS-BVOC emissions on O<sub>3</sub>  
110 concentrations, they did not investigate the impact of the UGS-LUCC effects.

111 Surface O<sub>3</sub> is generally formed through chemical reactions of VOCs and NO<sub>x</sub> in the presence of sunlight. The  
112 nonlinear correlation between O<sub>3</sub> and concentrations of BVOC and NO<sub>x</sub> underscores the importance of  
113 examining potential interactions between the UGS-BVOC emissions and anthropogenic emissions.  
114 Furthermore, recent studies have highlighted the significance of the UGS-LUCC effects and the UGS-BVOC  
115 emissions effects. Given the rise in urban O<sub>3</sub> pollution, investigating the influence of the UGS-LUCC effects  
116 and the UGS-BVOC emissions effects on O<sub>3</sub> can assist in rationalizing UGS planning and formulating air  
117 quality mitigation strategies. However, there is a lack of quantification regarding the combined effects of  
118 UGS-LUCC and UGS-BVOC emissions on O<sub>3</sub>.

120  
121 Situated in South China, Guangzhou (Figure 1) is one of the rapidly expanding cities in China since the  
122 initiation of the reform and opening-up policy, undergoing swift urbanization (Yao and Huang, 2023). Being  
123 a key city in the Guangdong-Hongkong-Macao Greater Bay Area, Guangzhou places significant emphasis on  
124 UGS development. In this study, we aim to reconstruct the leaf area index (LAI) dataset for urban areas and  
125 estimate the UGS-BVOC emissions utilizing the Model of Emissions of Gases and Aerosols from Nature  
126 version 3.1 (MEGANv3.1) (Guenther et al., 2020a). Subsequently, employing the Weather Research and  
127 Forecast model version 4.1.1 (WRFv4.1.1) (Salamanca et al., 2011) – Community Multiscale Air Quality  
128 model version 5.4 (CMAQv5.4) (<https://zenodo.org/record/7218076>, last accessed: June 3, 2023), we intend  
129 to estimate the improvements of the CMAQ simulation performance from considering UGS-LUCC and UGS-  
130 BVOC and investigate the UGS-LUCC effects, the UGS-BVOC emissions effects, and their combined  
131 impacts on O<sub>3</sub> over Guangzhou by configuring sensitivity cases.

## 132 **2. Methods and data**

### 133 **2.1 Leaf area index and land cover dataset**

134 The default LAI dataset to drive the MEGANv2.1 model which can be used for MEGANv3.1 is derived from the  
135 enhanced Moderate Resolution Imaging Spectroradiometer (MODIS) /MOD15A2H in 2003 with 1 km spatial  
136 resolution (Myndeni et al., 2015). As MODIS/MOD15A2H assigns an LAI value of 0 to urban areas,  
137 MEGANv3.1 compensates by averaging the LAI values in the vicinity of the urban area. However, this  
138 approach introduces considerable uncertainty in the estimation of UGS-BVOC emissions. Hence, we opted

139 for the Global Land Surface Satellite (GLASS) LAI product for MEGANv3.1 in 2017 with 500-m spatial  
140 resolutions, derived from MODIS surface reflectance data using the bidirectional long short-term memory  
141 (Bi-LSTM) model, which leverages existing global LAI products (Ma and Liang, 2022) and effectively  
142 incorporates the temporal and spectral information of MODIS surface reflectance. Consequently, the valid  
143 values of this data extend to urban areas, making it suitable for simulating the UGS-BVOC emissions.

144  
145 In this study, UGS are delineated as vegetation areas within the urban grid, and the urban grids are derived  
146 from MODIS/MCD12Q1 (Friedl and Sulla-Menashe, 2019) in 2017, which corresponds to the simulation  
147 period with 500 m spatial resolution. Furthermore, a high-resolution (10 m) land cover dataset in 2017 was  
148 also obtained from the Geographic Remote Sensing Ecological Network Platform (accessible at  
149 <http://www.gisrs.cn/infodata?id=1c089287-909e-4394-b07f-c7004be60884>, last accessed: 20/11/2023)  
150 and was employed to depict the spatial patterns of UGS. The processed land cover dataset is illustrated in  
151 Figure S1. Meanwhile, the use of high-resolution land use cover data is pivotal for accurately depicting the  
152 intricate details of land use cover, especially in areas broadly classified as urban by coarse-resolution data (i.e.,  
153 MCD12Q1) and this refined approach allows for a more precise differentiation of UGS. Specifically, we  
154 maintain a consistent urban area definition across both land use cover datasets, anchored by the urban  
155 delineation provided by the MCD12Q1 dataset. However, the coarse resolution of MCD12Q1 is insufficient  
156 for detailed spatial characterization of UGS. To address this limitation, we employ the high-resolution dataset  
157 to refine the characterization of non-urban surfaces within the urban boundaries (i.e., UGS) defined by  
158 MCD12Q1. This approach yields a sophisticated land cover dataset with 10 m spatial resolution that retains  
159 the urban extent delineated by MCD12Q1 while incorporating detailed representations of UGS absent in the  
160 original dataset. Consequently, while both datasets encompass identical urban extents, the default dataset lacks  
161 representations of UGS, in contrast to the high-resolution dataset, which includes detailed depictions of UGS.

## 162 2.2 MEGANv3.1 configuration

163 The calculation of BVOC emissions was performed utilizing MEGANv3.1 (accessible at  
164 <https://bai.ess.uci.edu/megan>, last accessed: 21 November 2023), which is a newly updated version.  
165 MEGANv3.1 estimates BVOC emissions as the product of an emission factor and an emission activity factor  
166 (Guenther et al., 2020a):

$$167 E = EF \times \gamma \quad (\text{Eq. 1})$$

168  
169 In this equation,  $E$  is the net emission flux ( $\mu\text{g m}^{-2} \text{h}^{-1}$ ), and  $\text{EF}$  is the weighted average of the emission  
170 factor ( $\mu\text{g m}^{-2} \text{h}^{-1}$ ) for each vegetation type calculated by Emission Factor Processor (EFP). The emission  
171 activity factor ( $\gamma$ ) considers emission responses to changes in environmental and phenological conditions.  
172 Compare with earlier versions,  $\gamma$  in MEGANv3.1 adds quantifications for responses to high and low  
173 temperature, high wind speed, and air pollution ( $\text{O}_3$ ).

$$\gamma = \text{LAI} \times \gamma_{TP} \times \gamma_{LA} \times \gamma_{SM} \times \gamma_{HT} \times \gamma_{LT} \times \gamma_{HW} \times \gamma_{CO_2} \times \gamma_{BD} \times \gamma_{O_3} \quad (\text{Eq. 2})$$

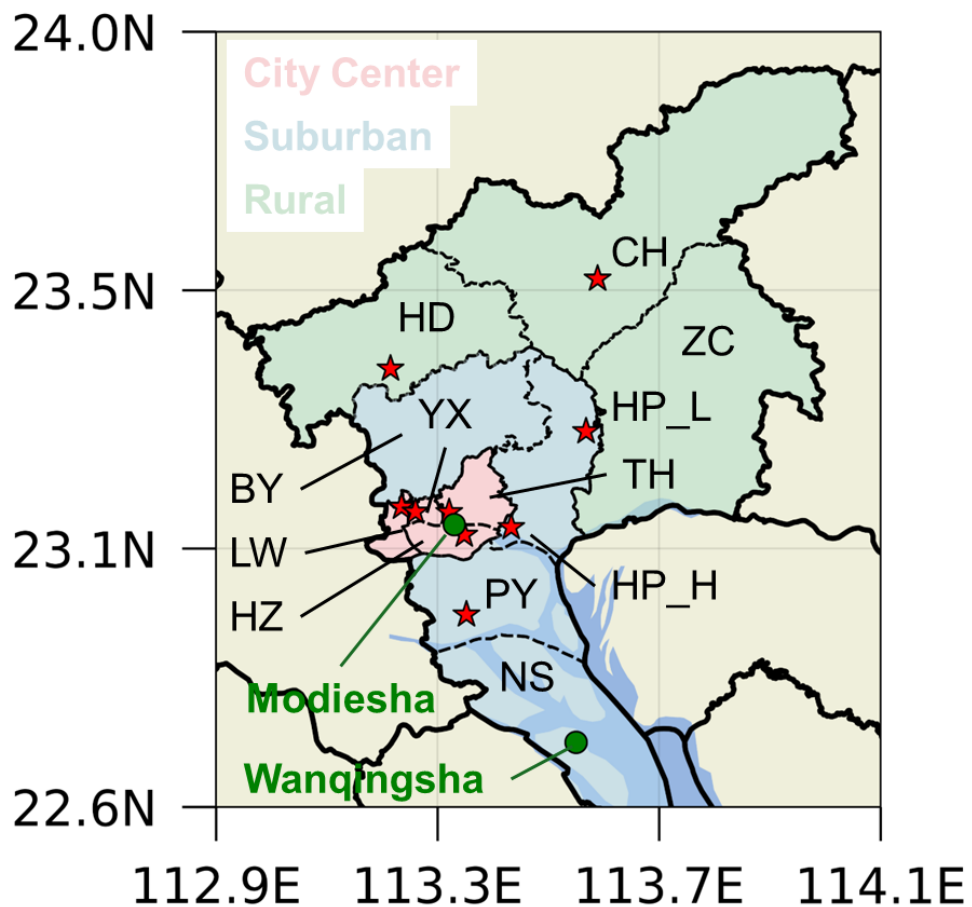
175  
176 In this equation, the activity factor denotes the emission response to canopy temperature/light( $\gamma_{TP}$ ), leaf age  
177 ( $\gamma_{LA}$ ), soil moisture ( $\gamma_{SM}$ ), high temperature ( $\gamma_{HT}$ ), low temperature ( $\gamma_{LT}$ ), high wind speed ( $\gamma_{HW}$ ), ambient  
178 CO<sub>2</sub> concentration ( $\gamma_{CO_2}$ ), bidirectional exchange ( $\gamma_{BD}$ ), O<sub>3</sub> exposure ( $\gamma_{O_3}$ ), and Leaf Area Index (LAI). In  
179 this study,  $\gamma_{CO_2}$  was not considered in the BVOC emission estimation. It is worth noting that MEGANv3.1  
180 uses the 2-m temperature variable from the WRF model to calculate BVOC emissions. Meanwhile, The  
181 MEGANv3.1 approach can calculate the emissions at each canopy level as the product of the emission  
182 factor and emission activity at each level.

183  
184 Hence, the input data to drive MEGANv3.1 comprises meteorological variables (e.g., temperature, solar  
185 radiation, relative humidity, soil moisture), LAI, and three types of land cover data (i.e., ecotype, growth  
186 form, and relative vegetation composition for each ecotype/growth form). Meanwhile, the growth form  
187 datasets in MEGANv3.1 contain considerations of evergreen broadleaf forests, grasslands, and crops, which  
188 cover all types of UGS in Guangzhou city (Figure S1). Meteorological data are obtained from the WRF  
189 simulation results, and the LAI dataset is detailed in Section 2.1 as well as additional default land cover data  
190 provided by MEGANv3.1 were employed.

## 191 **2.3 WRF-CMAQ and Case Configuration**

192 Both the WRFv4.1.1 model and the CMAQv5.4 model are compiled and operated on a server with a Linux  
193 environment. The WRFv4.1.1 model was employed to simulate meteorological conditions, utilizing initial and  
194 boundary conditions sourced from the NCEP 1° × 1° Final (FNL) reanalysis dataset (National Centers for  
195 Environmental Prediction, National Weather Service, NOAA, U.S. Department of Commerce, 2000). As

196 illustrated in Figure S2, four nested domains with horizontal resolutions of 27, 9, 3, and 1 km, respectively,  
197 were employed. The outermost domain encompasses mainland China, while the innermost domain zooms in  
198 Guangzhou city, and the physical parameterization configured for the WRF simulation is listed in Table S1.  
199 CMAQv5.4 utilized meteorological fields provided by WRF to model O<sub>3</sub> concentrations. The initial and  
200 boundary conditions for the CMAQ model were derived from the default profiles representing a clean  
201 atmosphere. In addition, we acquired anthropogenic emissions for the CMAQ domain from the Multi-  
202 resolution Emission Inventory for China (MEIC) 2017 developed by Tsinghua University, which contains  
203 monthly gridded (0.25° × 0.25°) emissions information for anthropogenic emissions. Moreover, the CMAQ  
204 model was configured with the Carbon Bond chemical mechanism (CB06) (Luecken et al., 2019) and AERO7  
205 (Pye et al., 2017). In this study, we incorporated the Modular Emission Inventory Allocation Tools for the  
206 Community Multiscale Air Quality model (MEIAT-CMAQ, <https://github.com/Airwhf/MEIAT-CMAQ>, last  
207 accessed: February 27, 2024) to allocate spatial and species-specific emissions within the raw inventories,  
208 addressing discrepancies in resolution and species compared to the modeled configurations. Moreover,  
209 MEIAT-CMAQ can directly generate the hourly model-ready emission files for CMAQ via temporal  
210 allocation. The model simulation spanned a month, from 21 August 2017 to 30 September 2017. To mitigate  
211 bias resulting from meteorological and chemical drift, the initial 10 days of this simulation were designated  
212 as spin-up and were not included in the analysis for this study. Given the spatial heterogeneity in the  
213 distribution of UGS across different areas, this study categorizes Guangzhou into city center, suburban, and  
214 rural regions (Figure 1). Specifically, the city center areas comprise Haizhu (HZ), Liwan (LW), Yuexiu (YX),  
215 and Tianhe (TH) districts. The city center region has more UGS areas due to the higher urban land use and  
216 land cover fraction (Figure S1) compared to the suburban and rural regions. The suburban areas encompass  
217 Huangpu (HP), Baiyun (BY), Panyu (PY), and Nansha (NS) districts. Lastly, the rural regions include  
218 Zengcheng (ZC), Conghua (CH), and Huadu (HD) districts. To facilitate clear differentiation between the two  
219 sites in the HP region, they have been designated as HP\_L and HP\_H, respectively.



220  
221 **Figure 1** The innermost domain of WRF-CMAQ with various areas and the air quality station locations map. Modiesha and Wanqingsha  
222 are the observation sites for isoprene.  
223

224 In this study, four distinct cases, as listed in Table 1 were established to investigate the impacts of UGS-LUCC,  
225 UGS-BVOC, and their combined effects on the ozone simulation. These cases also focused on the performance  
226 of the CMAQ simulation and the influence on  $O_3$  episodes. The Gdef\_N case considered as the base case,  
227 employs default land use cover data—specifically, data excluding UGS, and uses the LAI dataset with urban  
228 areas omitted (N-LAI). In contrast, the Gdef\_Y case is similar to Gdef\_N but incorporates the LAI dataset that  
229 includes urban areas (T-LAI). This adjustment allows for the assessment of the UGS-BVOC emission effects  
230 on  $O_3$  concentrations. The Ghr\_N case mirrors Gdef\_N but differs by integrating high-resolution land use  
231 cover data, which encompasses UGS land use cover. This case aims to examine the UGS-LUCC effects on  $O_3$   
232 concentrations. Finally, the Ghr\_Y case combines high-resolution land use cover data with the LAI dataset  
233 inclusive of urban areas, thereby enabling an exploration of the combined effects of UGS-BVOC emissions  
234 and UGS-LUCC on  $O_3$  concentrations.  
235  
236

237  
238

Table 1 Case configurations

| Name   | LC dataset           | LAI dataset | Description      |
|--------|----------------------|-------------|------------------|
| Gdef_N | Default data         | N-LAI       | Base             |
| Gdef_Y | Default data         | T-LAI       | UGS-BVOC effects |
| Ghr_N  | High-resolution data | N-LAI       | UGS-LUCC effects |
| Ghr_Y  | High-resolution data | T-LAI       | combined effects |

239 **2.4 Observation Dataset**

240 We use the hourly ground-level meteorological observations, encompassing 2-m temperature (T2) and 10-m  
 241 wind speed (WS10), sourced from national basic meteorological stations provided by the Guangdong  
 242 Provincial Meteorological Service (Figure S3). Hourly ambient concentrations of O<sub>3</sub>, CO, and NO<sub>2</sub> from  
 243 national monitoring stations are gathered from the China National Environmental Monitoring Centre  
 244 (CNEMC; <http://www.cnemc.cn>, last assess: 24 December 4, 2024). The real-time hourly concentration of  
 245 O<sub>3</sub> was measured by the ultraviolet absorption spectrometry method and differential optical absorption  
 246 spectroscopy at each monitoring site. NO<sub>2</sub> concentrations are measured by the molybdenum converter method  
 247 known to have positive interferences from NO<sub>2</sub> oxidation products (Dunlea et al., 2007). The instrumental  
 248 operation, maintenance, data assurance, and quality control were properly conducted based on the most recent  
 249 revisions of China Environmental Protection Standards (Zhang and Cao, 2015), and the locations of these air  
 250 quality stations are depicted in Figure 1. Additionally, meteorological data also undergo thorough quality  
 251 control. Subsequently, they are utilized to assess the model performance of WRF-CMAQ.

252  
 253 For the isoprene (ISOP) evaluation, we use observation data from the Modiesha (23.11°N, 113.33°E) and  
 254 Wanqingsha (22.71°N, 113.55°E) sites (Figure 1), where an online gas chromatography-mass  
 255 spectrometry/flame ionization detector system (GC-FID/MSD, TH 300B, Wuhan) is used to measure VOCs  
 256 in the ambient atmosphere. The system has a sampling rate of 60 mL/min for 5 minutes per sample, with a  
 257 sampling frequency of once per hour (Meng et al., 2022). The ISOP observation data undergo rigorous quality  
 258 control, which can be used for evaluating simulated ISOP concentrations. It is worth noting that the ISOP  
 259 observational data for the Modiesha site covers September 2017, while the Wanqingsha site has data coverage  
 260 from September 7 to September 30, 2017.

261 **3. Results and discussion**

262 **3.1 Model Evaluation**

263 Evaluation of the WRF-CMAQ model performance is undertaken through comparison against ground-level  
264 observations and the evaluation metrics of meteorological parameters are listed in Table S2, which shows that  
265 the meteorological fields were faithfully reproduced in this study and can be used to drive the air quality model.

266  
267 ISOP and monoterpene (TERP) are the major species of BVOC emission, making their concentration  
268 assessment a feasible and convincing method for indirectly validating the accuracy of BVOC emission  
269 estimates. BVOCs are the major sources of ISOP and monoterpene (TERP), rendering the assessment of their  
270 concentrations a pivotal method for indirectly verifying the accuracy of BVOC emission estimates. Table 2  
271 delineated within this study presents the mean concentrations of ISOP derived from various cases juxtaposed  
272 with the observed average concentrations. This comparative analysis in the Modiesha site reveals that after  
273 the incorporation of the UGS-BVOC emissions, there is an augmentation in the ISOP concentration from 0.29  
274 to 0.35 ppb and from 0.23 to 0.29 ppb under distinct land use cover cases (Gdef and Ghr), relative to an  
275 observed concentration of 0.34 ppb. Meanwhile, the evaluation at the Wanqingsha site, where the observed  
276 mean ISOP concentration was 0.45 ppb from September 7 to September 30, 2017, shows that the modeled  
277 ISOP concentrations increased from 0.29 to 0.31 ppb and from 0.27 to 0.29 ppb under distinct land use cover  
278 cases (Gdef and Ghr) when UGS-BVOC emissions were included. Additionally, all cases successfully capture  
279 the hourly ISOP concentrations when compared to observations at both the Modiesha and Wanqingsha sites  
280 (Figure S4). This increment signifies a substantial diminution in the discrepancy between the modeled and  
281 observed concentrations attributable to the UGS-BVOC emissions. Analogously, the integration of the UGS-  
282 BVOC emissions yields a refinement in the estimation accuracy of ISOP concentrations at the Modiesha site,  
283 as evidenced by a reduced bias.

284  
285 These findings reveal that ISOP concentrations are underestimated by 16.4% and 34.7% in the Modiesha and  
286 Wanqingsha sites when UGS-BVOCs are excluded, respectively, suggesting the important role of UGS-  
287 BVOCs emissions in modeling. Moreover, numerous studies highlight the significant role of ISOP in  $O_3$   
288 formation within the Pearl River Delta (PRD) region, including Guangzhou. For instance, Zheng et al., (2009)  
289 demonstrated that ISOP has the highest ozone formation potential among all VOCs. Therefore, incorporating

290 UGS-BVOCs into ISOP concentration estimates is crucial for accurately modeling regional O<sub>3</sub> levels.

291  
292 **Table 2 The evaluation results for the monthly mean ISOP concentrations. The “Gdef\_N”, “Gdef\_Y”, “Ghr\_N”, and “Ghr\_Y” columns**  
293 **show the various metrics from comparing the hourly observation and simulation values during September 2017 for the Modiesha site and**  
294 **7 September 2017 to 30 September 2017 for the Wanqingsha site.**

| Site name  | Metrics | Gdef_N (ppb) | Gdef_Y (ppb) | Ghr_N (ppb) | Ghr_Y (ppb) |
|------------|---------|--------------|--------------|-------------|-------------|
| Modiesha   | Sim.    | 0.29         | 0.35         | 0.23        | 0.29        |
|            | Obs.    | 0.34         | 0.34         | 0.34        | 0.34        |
|            | MB      | -0.06        | 0.01         | -0.11       | -0.05       |
|            | NME     | 76.0%        | 68.7%        | 73.6%       | 66.2%       |
|            | NMB     | -16.4%       | 3.5%         | -31.3%      | -13.1%      |
|            | R       | 0.44         | 0.46         | 0.37        | 0.39        |
| Wanqingsha | Sim.    | 0.29         | 0.31         | 0.27        | 0.29        |
|            | Obs.    | 0.45         | 0.45         | 0.45        | 0.45        |
|            | MB      | -0.15        | -0.14        | -0.17       | -0.15       |
|            | NME     | 58.9%        | 56.8%        | 60.4%       | 58.1%       |
|            | NMB     | -34.7%       | -30.6%       | -38.7%      | -34.8%      |
|            | R       | 0.35         | 0.39         | 0.34        | 0.4         |

295  
296 Additionally, various statistical metrics were used to assess the performance of hourly O<sub>3</sub>, MDA8 O<sub>3</sub>, and NO<sub>2</sub>  
297 concentrations from the CMAQ simulation (Emery et al. 2017). These metrics comprise the correlation  
298 coefficient (R), normalized mean bias (NMB), and normalized mean error (NME). The formulas for these  
299 metrics are listed in Table S3. As shown in Table 3, the modeling performance for all cases are reasonable,  
300 albeit with some degree of underestimation. Despite these discrepancies, the model demonstrates sufficient  
301 reliability and can be effectively used in the subsequent study. Meanwhile, the MBs of MDA8 O<sub>3</sub> across  
302 various cases indicate a substantial improvement in the CMAQ simulation when UGS-BVOC, UGS-LUCC,  
303 and their combined effects are considered. Specifically, the MB values of MDA8 O<sub>3</sub> decrease from -2.16 ppb  
304 in the Gdef\_N case to -0.26 ppb in the Ghr\_Y case, demonstrating that incorporating UGS-BVOC, UGS-  
305 LUCC, and their combined effects can enhance the accuracy of predicted daytime O<sub>3</sub> concentrations. In  
306 addition, we also evaluate the simulation performance for NO<sub>2</sub> in each case and the results suggest that all  
307 models have R above 0.63, and while there is some overestimation, the NMB is 15.0%, 15.2%, 13.0%, and  
308 13.2% for Gdef\_N, Gdef\_Y, Ghr\_N, and Ghr\_Y, respectively. It should be emphasized that integrating UGS-  
309 BVOC into the modeling process can slightly improve the accuracy of NO<sub>2</sub> predictions, reducing the MB from  
310 3.27 to 3.24 ppb, and from 2.84 to 2.81 ppb for Gdef and Ghr cases, respectively. The improvement in NO<sub>2</sub>  
311 predictions is attributed to the increased involvement inclusion of NO<sub>2</sub> in O<sub>3</sub> formation caused by the UGS-  
312 BVOC emissions in the CMAQ model, which reduces enhances NO<sub>2</sub> involvement in O<sub>3</sub> formation. This

313 process leads to lower simulated NO<sub>2</sub> concentrationsand narrows its bias against, reducing the  
 314 observationMBs compared to observations.

315  
 316  
 317 **Table 3 Evaluation results of the simulated monthly mean hourly O<sub>3</sub>, MDA8 O<sub>3</sub>, and hourly NO<sub>2</sub> mixing ratios for each case during**  
 318 **September 2017.**

| Pollutant              | Case name | Sim (ppb) | Obs (ppb) | MB (ppb) | NMB    | NME    | R    |
|------------------------|-----------|-----------|-----------|----------|--------|--------|------|
| Hourly O <sub>3</sub>  | Gdef_N    | 28.23     | 30.49     | -2.26    | -6.7%  | 23.6%  | 0.82 |
|                        | Gdef_Y    | 28.67     | 30.49     | -1.82    | -5.3%  | 23.6%  | 0.82 |
|                        | Ghr_N     | 28.89     | 30.49     | -1.60    | -4.8%  | 22.5%  | 0.83 |
| MDA8 O <sub>3</sub>    | Ghr_Y     | 29.33     | 30.49     | -1.15    | -3.4%  | 22.4%  | 0.83 |
|                        | Gdef_N    | 60.11     | 62.27     | -2.16    | -3.47% | 21.71% | 0.84 |
|                        | Gdef_Y    | 61.04     | 62.27     | -1.23    | -1.97% | 21.40% | 0.84 |
| Hourly NO <sub>2</sub> | Ghr_N     | 61.07     | 62.27     | -1.20    | -1.92% | 21.28% | 0.84 |
|                        | Ghr_Y     | 62.00     | 62.27     | -0.26    | -0.42% | 21.23% | 0.84 |
|                        | Gdef_N    | 24.78     | 21.50     | 3.27     | 15.2%  | 45.7%  | 0.63 |
| Hourly NO <sub>2</sub> | Gdef_Y    | 24.74     | 21.50     | 3.24     | 15.0%  | 45.5%  | 0.63 |
|                        | Ghr_N     | 24.35     | 21.50     | 2.84     | 13.2%  | 43.8%  | 0.63 |
|                        | Ghr_Y     | 24.32     | 21.50     | 2.81     | 13.0%  | 43.6%  | 0.63 |

319  
 320 In terms of O<sub>3</sub>, the UGS-BVOC, UGS-LUCC, and their combined effects have various performances in  
 321 different regions (Table 4). These results indicate that the inclusion of UGS-BVOC emissions  
 322 remarkably significantly influences MDA8 O<sub>3</sub> and hourly O<sub>3</sub> concentrations in the city center region and this  
 323 effect, primarily observed when comparing the Gdef\_Y with Gdef\_N and Ghr\_Y with Ghr\_N cases, is largely  
 324 due to the VOC-limited areas prevalent in Guangzhou (He et al., 2024). By integrating the UGS-BVOC  
 325 emissions and UGS-LUCC into the models (comparing Gdef\_Ghr\_Y and Gdef\_N cases), the MBs of MDA8  
 326 O<sub>3</sub> and hourly O<sub>3</sub> in all regions, including a notable improvement in the city center region from -3.6263 to -  
 327 0.75 ppb and -2.86 to -1.1852 ppb, respectively, is reduced. Additionally, the UGS-BVOC emissions slightly  
 328 enhance R values of MDA8 O<sub>3</sub> and hourly O<sub>3</sub> in the city center and suburban regions, indicating a more  
 329 accurate the daytime trend and the diurnal cycle representation, respectively. The UGS-LUCC effects, as seen  
 330 when comparing Ghr\_N and Gdef\_N cases, also greatly improve model biases and the combined effects of  
 331 both UGS-BVOC and UGS-LUCC (comparing the Ghr\_Y and Gdef\_N cases) substantially ameliorate model  
 332 biases in the city center and suburban regions.

333 **Table 4 Evaluation results of simulated monthly mean hourly O<sub>3</sub> and MDA8 O<sub>3</sub> mixing ratios in city center, suburban, and rural areas**  
 334 **for each case during September 2017.**

| Variable | Regions | MB (ppb) | R |
|----------|---------|----------|---|
|----------|---------|----------|---|

|                       |             | Gdef_N          | Gdef_Y          | Ghr_N           | Ghr_Y            | Gdef_N         | Gdef_Y         | Ghr_N           | Ghr_Y          |
|-----------------------|-------------|-----------------|-----------------|-----------------|------------------|----------------|----------------|-----------------|----------------|
| MDA8 O <sub>3</sub>   | City center | -3.6 <u>327</u> | -2.24 <u>4</u>  | -2.11 <u>0</u>  | -0.7 <u>547</u>  | 0.8 <u>105</u> | 0.81 <u>0</u>  | 0.81 <u>0</u>   | 0.81 <u>3</u>  |
|                       | Suburban    | -4.0 <u>876</u> | -3.25 <u>4</u>  | -3.21 <u>0</u>  | -2.3 <u>876</u>  | 0.7 <u>437</u> | 0.74 <u>3</u>  | 0.7 <u>217</u>  | 0.7 <u>327</u> |
|                       | Rural       | -5.1 <u>109</u> | -4.7 <u>657</u> | -4.8 <u>766</u> | -4.5 <u>328</u>  | 0.6 <u>765</u> | 0.6 <u>655</u> | 0.7 <u>0695</u> | 0.69 <u>0</u>  |
| Hourly O <sub>3</sub> | City center | -2.86 <u>2</u>  | -2.29 <u>2</u>  | -2.09 <u>86</u> | -1.52 <u>0</u>   | 0.80 <u>0</u>  | 0.80 <u>2</u>  | 0.81 <u>4</u>   | 0.81 <u>2</u>  |
|                       | Suburban    | -3.1 <u>548</u> | -2.80 <u>3</u>  | -2.6 <u>547</u> | -2.30 <u>295</u> | 0.82 <u>4</u>  | 0.83 <u>25</u> | 0.82 <u>4</u>   | 0.83 <u>26</u> |
|                       | Rural       | -1.18 <u>4</u>  | -1.63 <u>0</u>  | -1.3 <u>875</u> | -1.16 <u>4</u>   | 0.74 <u>2</u>  | 0.74 <u>4</u>  | 0.75 <u>4</u>   | 0.75 <u>0</u>  |

### 3.2 Estimation of UGS-BVOC emissions under different land use cover

This study comprehensively summarizes the UGS-BVOC emissions across various species for all regions in Guangzhou City in September. Given that the variances in the UGS-BVOC emissions due to different land use covers are relatively minor, the primary Table 5 presents emissions driven by the default land use cover. For a detailed breakdown of emissions attributable to varied land use covers, refer to Table S4. A review of the data reveals that TERP and ISOP rank as the highest emitting species with proportions are 20.46% and 31.91% in this study, respectively, aligning with the findings of previous studies (Cao et al., 2022; Guenther et al., 2012b). Furthermore, Table 5 reveals that in September, the UGS-BVOC emissions in Guangzhou amounted to 666 Gg (~90 Mg/km<sup>2</sup>), with ISOP and TERP contributing remarkably to the total UGS-BVOC emissions. In comparison to anthropogenic VOC (AVOC) and BVOC emissions, UGS-BVOC emissions account for approximately 33.45% in the city center region. Regionally, the suburban region registered the highest UGS-BVOC emissions in Guangzhou, peaking at 367 Gg. This is followed closely by the rural and city center regions, recording emissions of 173174 Gg and 125126 Gg, respectively.

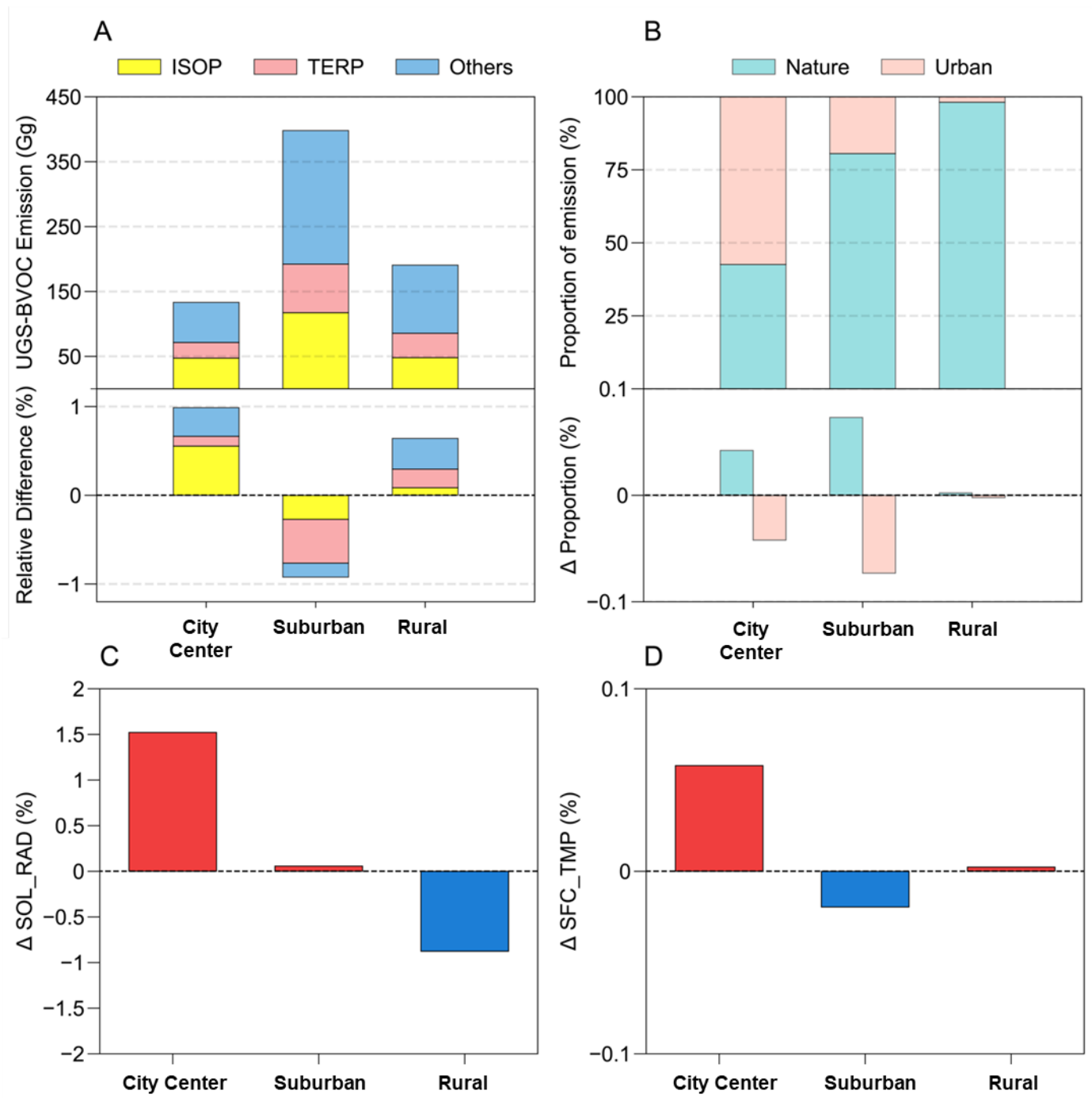
Table 5 The summarized table of UGS-BVOC emissions in Guangzhou city in September 2017 via default land use cover (units: Gg).

| Species      | Abbreviations | City center (Gg) | Suburban (Gg) | Rural (Gg) | Total (Gg) |
|--------------|---------------|------------------|---------------|------------|------------|
| Acetic acid  | AACD          | 0.86             | 2.44          | 1.18       | 4.48       |
| Acetaldehyde | ALD2          | 3.46             | 11.57         | 5.83       | 20.86      |
| Formaldehyde | FORM          | 0.95             | 3.90          | 2.17       | 7.02       |
| Methanol     | MEOH          | 12.47            | 41.31         | 20.36      | 74.14      |
| Formic acid  | FACD          | 2.79             | 7.84          | 3.79       | 14.42      |
| Ethane       | ETHA          | 2.12             | 8.40          | 4.64       | 15.16      |
| Ethanol      | ETOH          | 3.63             | 12.13         | 6.11       | 21.87      |
| Acetone      | ACET          | 6.22             | 21.52         | 11.63      | 39.37      |
| Propane      | PRPA          | 2.08             | 8.21          | 4.54       | 14.83      |
| Ethene       | ETH           | 3.97             | 15.64         | 8.64       | 28.25      |
| Isoprene     | ISOP          | 47.30            | 117.32        | 48.06      | 212.68     |
| Monoterpenes | TERP          | 24.07            | 74.85         | 37.51      | 136.43     |

|                |       |        |        |        |        |
|----------------|-------|--------|--------|--------|--------|
| Alpha pinene   | APIN  | 11.26  | 30.07  | 13.16  | 54.49  |
| Methane        | ECH4  | 0.04   | 0.14   | 0.08   | 0.26   |
| Sesquiterpenes | SESQ  | 4.31   | 11.97  | 5.95   | 22.23  |
| Total          | Total | 125.53 | 367.31 | 173.65 | 666.49 |

Figure 2A provides a detailed illustration of the UGS-BVOC emissions across various regions in Guangzhou City, driven by default land use cover data, and compares these with the estimates derived from high-resolution land use cover data, which presents that the suburban region exhibits the highest UGS-BVOC emissions among the three studied regions, totaling 413.47 Gg. This predominance is linked to the larger extent of UGS in the suburban region, as depicted in Figure 5A, while the emissions in the city center and rural regions are reported at 137.69 Gg and 198.64 Gg, respectively. Moreover, UGS-LUCC is instrumental in modulating BVOC emissions, leading to an uptick in the city center and rural regions while precipitating a decline in the suburban region. Notably, a slight increase in solar radiation (SOL\_RAD) by 0.05% (Figure 2C), attributable to a reduced urban fraction in the Ghr dataset, results in augmented solar exposure. Concurrently, a marginal reduction in surface temperature (SFC\_TMP) by 0.02% (Figure 2D), facilitated by increased vegetation albedo cooling effects, underpins the decrease in UGS-BVOC emissions within suburban regions. This phenomenon underscores the critical role of lowered SFC\_TMP—driven by vegetation's higher albedo—in curtailing emissions stemming from UGS-LUCC. [Temperature-dependent BVOC emissions are among the well-known key temperature-dependent mechanisms influencing ozone levels, alongside other processes including changes in chemical reaction rates, soil NOx emissions, dry deposition, and PAN decomposition, as demonstrated in Li et al. \(2024\).](#) Moreover, in the city center contexts, the diminished urban fraction enhances SOL\_RAD and SFC\_TMP, promoting higher emissions, a trend mirrored to a lesser extent in the rural region following the update of land use cover data to Ghr. Figure 2B offers a clear depiction of the proportion of UGS-BVOC emissions relative to non-UGS area BVOC emissions in each region of Guangzhou City, which presents that the UGS-BVOC emissions in the city center region constitute 57.34% of the total BVOC emissions in this region because of the larger urban proportions in the city center region (Figure 5), while the UGS-BVOC emission proportion in suburban and rural are 19.44% and 1.86% respectively. This indicates a significant contribution of the UGS-BVOC emissions in the the city center region. Furthermore, when examining the relative differences in the BVOC emissions resulting from various land use covers across the city, the changes are found to be minimal, which suggests that meteorological alterations from land use cover do not majorly influence the proportion of the UGS-BVOC emissions emanating in Guangzhou. Thus, factors other than land use changes might be more critical in shaping the distribution and intensity of the UGS-BVOC

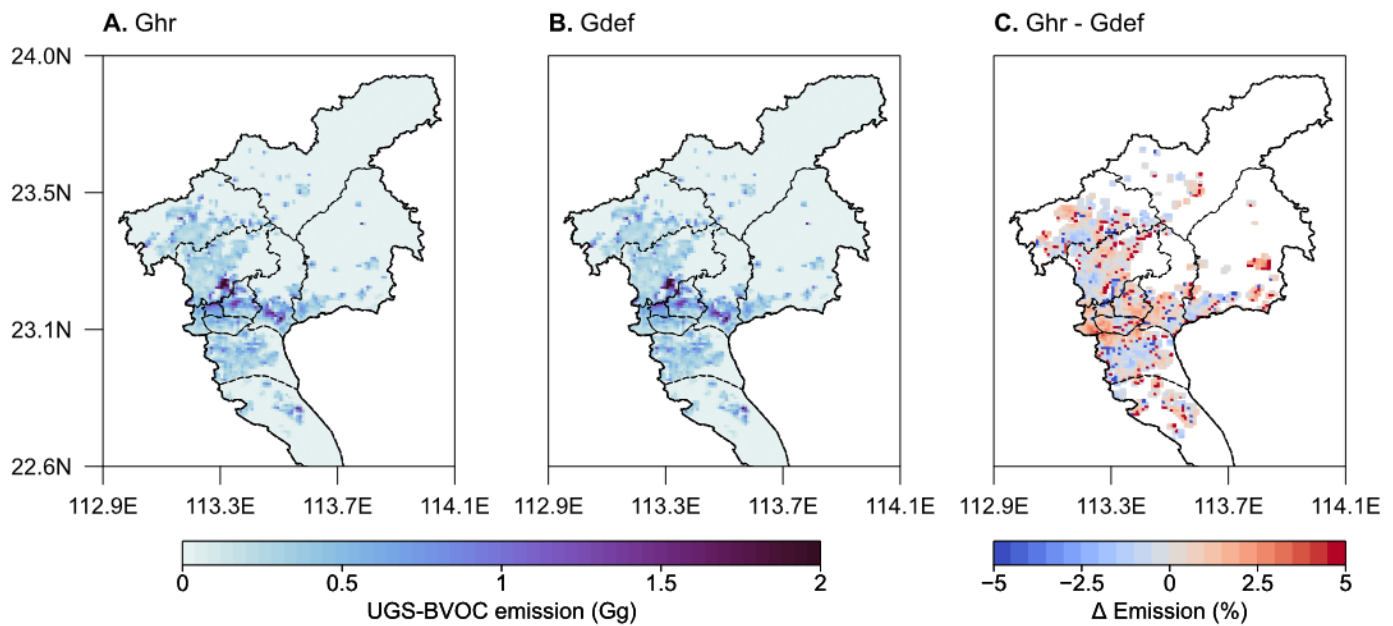
378 emissions in urban settings.



379  
380 **Figure 2** The UGS-BVOC emissions of each species and relative difference (Ghr - Gdef) from various land use cover (a), the proportion  
381 of emissions from urban and nature and the relative proportion difference (Ghr - Gdef) from various land use cover (b), the relative  
382 difference of solar radiation (C), and surface temperature (D) driven via various land use cover datasets. All values in these figure are  
383 during September 2017.  
384

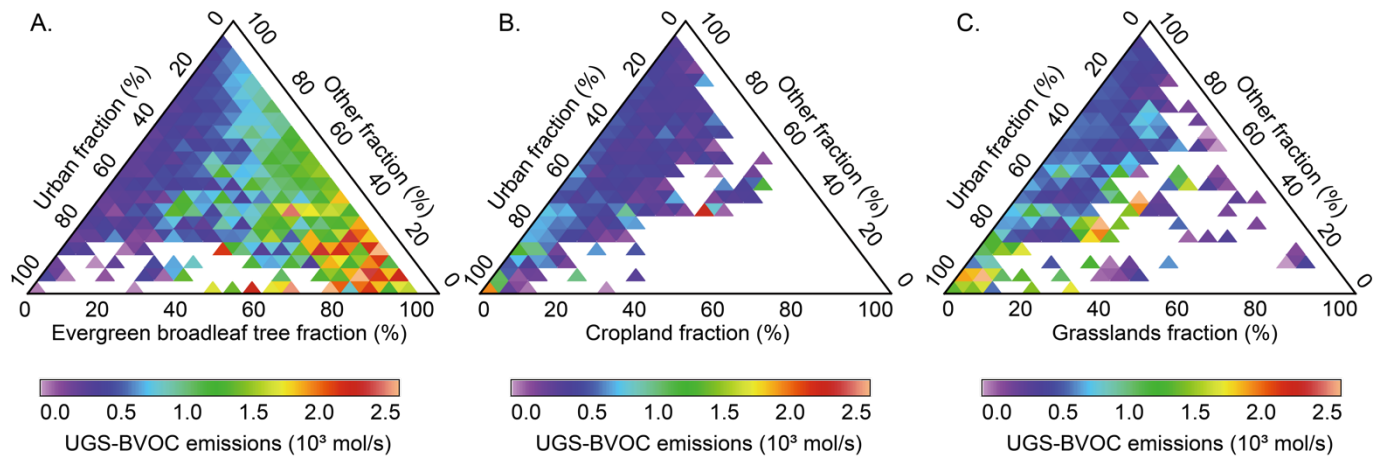
385 Figure 3A-B collectively highlight the patterns of the UGS-BVOC emissions across different land use covers,  
386 pinpointing the emission hotspots in city center and suburban regions, which effectively illustrate how land  
387 use cover influences the UGS-BVOC emissions in various parts of the city. Additionally, Figure 3C delves  
388 into the disparities in the UGS-BVOC emissions attributed to different land use cover datasets. It reveals that

389 the variations in emissions are predominantly concentrated in the identified hotspots. Moreover, Figure 3-C  
 390 indicates that employing high-resolution land cover data typically results in marginally higher estimates of the  
 391 UGS-BVOC emissions, with an increase ranging between 0.8% to 2.9%. Figure 5E-F illustrate that despite a  
 392 marginal reduction in solar radiation within the city center region, a corresponding minor temperature  
 393 elevation modestly boosts UGS-BVOC emissions, which presents that the increase in temperature from UGS-  
 394 LUCC causes the rise of the UGS-BVOC emissions.



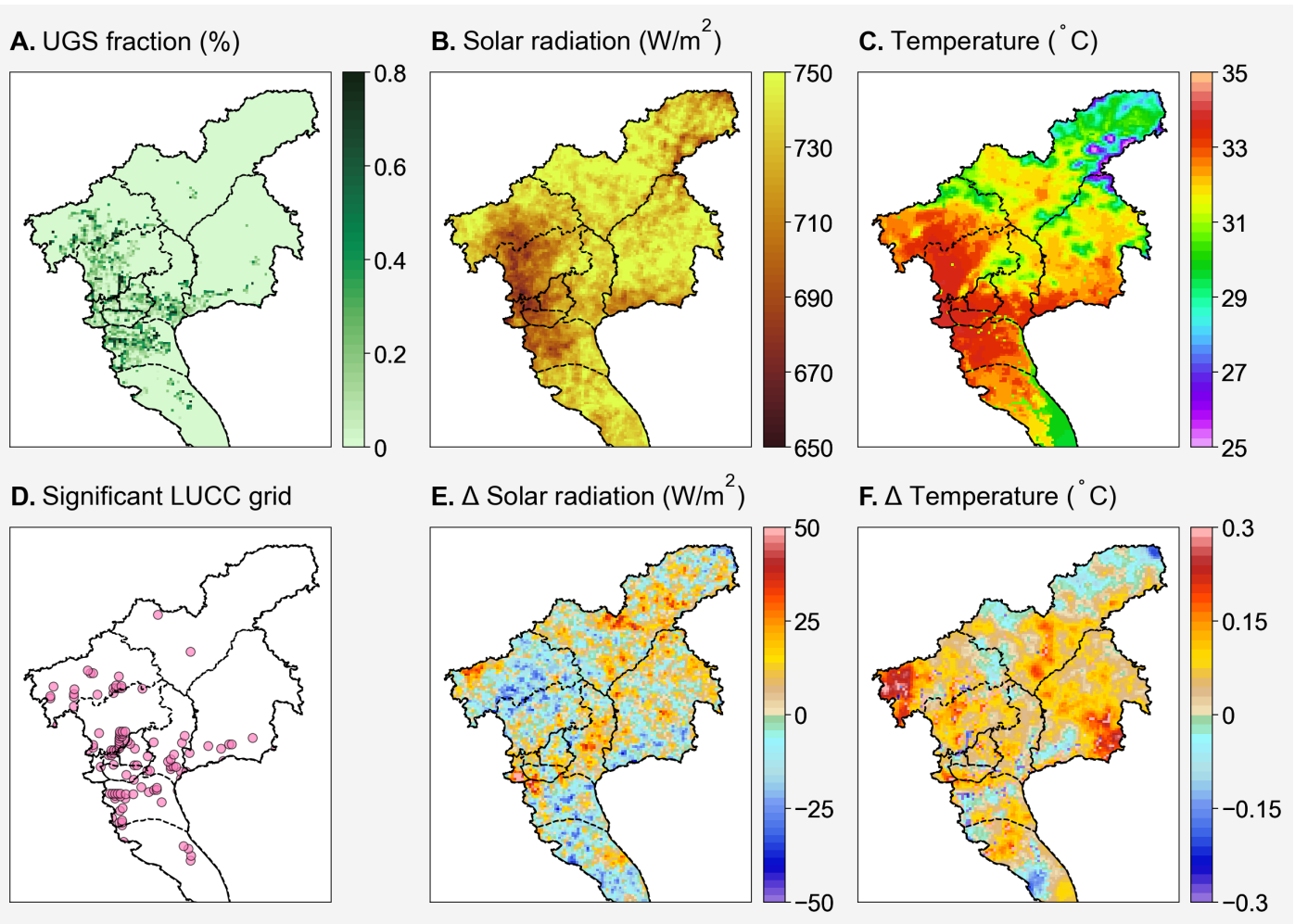
395  
 396 **Figure 3** The UGS-BVOC emission maps in September 2017 from default (A) and high-resolution (B) land use cover, and the differences  
 397 of various UGS-BVOC emissions (C).

398 As illustrated in Figure S1, UGS in Guangzhou comprises three primary types of vegetation: evergreen  
 400 broadleaf forests, which are composed of Evergreen Broadleaf Trees (EBTs), cropland, and grasslands. This  
 401 classification has enabled a more nuanced understanding of how different types of UGS vegetation influence  
 402 UGS-BVOC emissions. Figure 4 reveals that EBTs predominate the urban vegetation landscape in Guangzhou  
 403 and are associated with higher rates of UGS-BVOC emissions as their coverage increases. Conversely, an  
 404 increase in the proportion of cropland correlates with reduced UGS-BVOC emissions, highlighting its minimal  
 405 contribution to the overall UGS-BVOC emissions of Guangzhou. Grasslands exhibit a variable impact on  
 406 BVOC emissions; when they constitute over 80% of the UGS, the emission rates are relatively low. However,  
 407 when grassland coverage ranges between 60-80%, its BVOC emissions surpass those from cropland within  
 408 the same percentage range. Overall, EBTs emerge as the primary contributors to UGS-BVOC emissions, with  
 409 grasslands and croplands making lesser contributions.



410  
411 **Figure 4 Ternary heat map for various vegetation in UGS with the UGS-BVOC emission rate and the invalid value in this figure represents**  
412 **no UGS-BVOC emission.**

413  
414 In addition to the proportion of UGS, the UGS-BVOC emissions in Guangzhou city are significantly  
415 influenced by meteorological factors such as surface temperature and solar radiation (Guenther et al., 2020b).  
416 To elucidate the spatial heterogeneity of the UGS-BVOC emissions, this study analyzes variations in these  
417 key factors. The simulation results depicted in Figure 5A show the distribution pattern of UGS, which are  
418 predominantly located in the city center region, which account for a higher percentage of the UGS-BVOC  
419 emissions compared to others. Interestingly, as indicated in Figure 5B, the city center region receives less solar  
420 radiation than other regions likely due to the shading effect of urban canopies. Conversely, the city center  
421 region exhibits elevated temperatures attributable to the urban heat island effect, leading to an increase in  
422 UGS-BVOC emissions. Thus, while the distribution of UGS contributes to the variation in the UGS-BVOC  
423 emissions across different regions, the more significant factor is the enhanced UGS-BVOC emission due to  
424 higher temperatures in densely urbanized areas. The spatial dynamics of the UGS-BVOC emissions are  
425 significantly shaped by two key meteorological factors: solar radiation and surface temperature. These  
426 elements independently play a crucial role in determining both the spatial pattern and the intensity of the UGS-  
427 BVOC emissions. Solar radiation directly influences the rate of photosynthesis and, consequently, the  
428 production of BVOCs, while temperature affects not only the physiological processes of vegetation but also  
429 the volatilization rate of these compounds (Fuhrer et al., 1997; Lombardozzi et al., 2015). The intricate  
430 interplay between these factors leads to spatial variations in the UGS-BVOC emissions, with areas receiving  
431 higher solar radiation and experiencing warmer temperatures typically exhibiting more intense BVOC  
432 emissions.



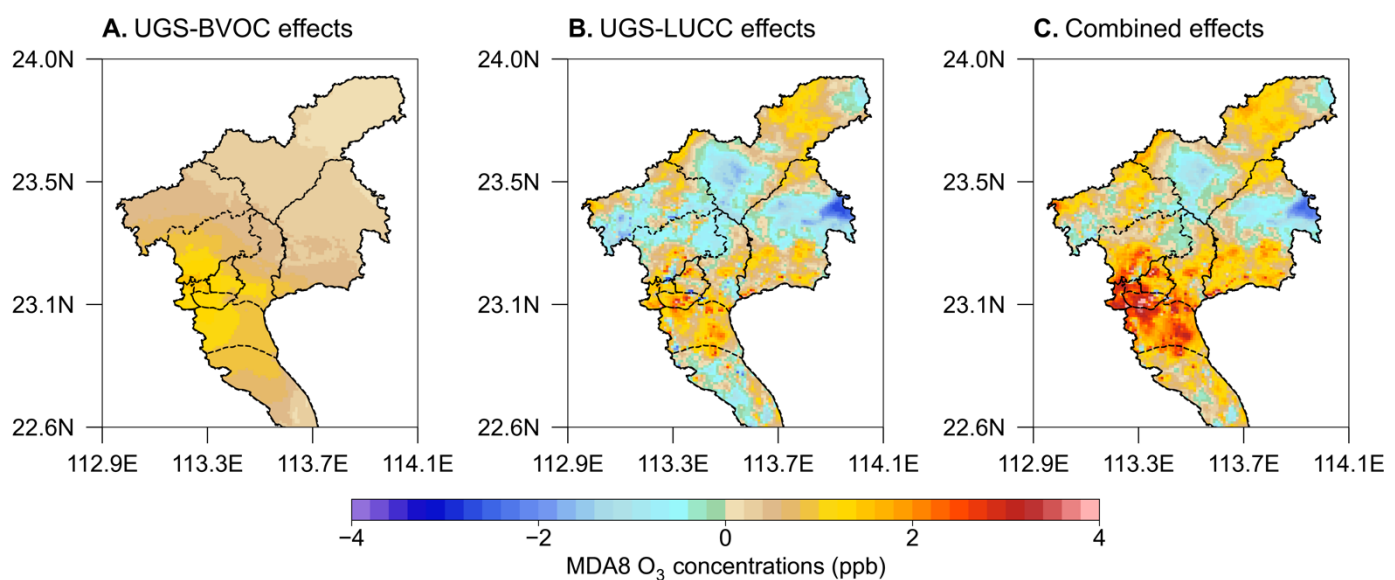
433  
434 **Figure 5** The UGS map (A) and the meteorological fields during September 2017 from the Ghr\_N case (B and C). (D) is the grid locations  
435 where the land use experienced significant changes, (E) and (F) are the differences in solar radiation and temperature during the analysis  
436 periods (1 September 2017 to 30 September 2017) in various land use cover data (Ghr - Gdef).

437 This section has conclusively demonstrated that during the high O<sub>3</sub> season (September) in Guangzhou, the  
438 contribution of UGS-BVOC is substantial and cannot be overlooked and a notable finding is the strong spatial  
439 heterogeneity in these emissions across the city. The analysis also highlights high-resolution land use cover  
440 data increase the estimation of the UGS-BVOC emissions in the city center region.

### 441 3.3 Impact of UGS-LUCC and UGS-BVOC on Ozone Concentrations

442 The study evaluates the effects of UGS-BVOC and UGS-LUCC on MDA8 O<sub>3</sub> concentrations in Guangzhou,  
443 both individually and in combination. Figure 6 presents the absolute contributions from various cases, while  
444 the relative differences are shown in Figure S4S5. The analysis reveals that the UGS-BVOC emissions alone  
445 (Figure 6A) primarily affect the city center region, greatly increasing MDA8 O<sub>3</sub> concentrations by 1.0-1.4 ppb  
446 (+2.3-3.2%), which increment aligns with findings from Los Angeles, where Schlaerth et al., (2023) reported  
447 a contribution of 1.2 ppb from UGS-BVOC to urban MDA8 O<sub>3</sub> levels. N. Wang et al. (2019) reported that

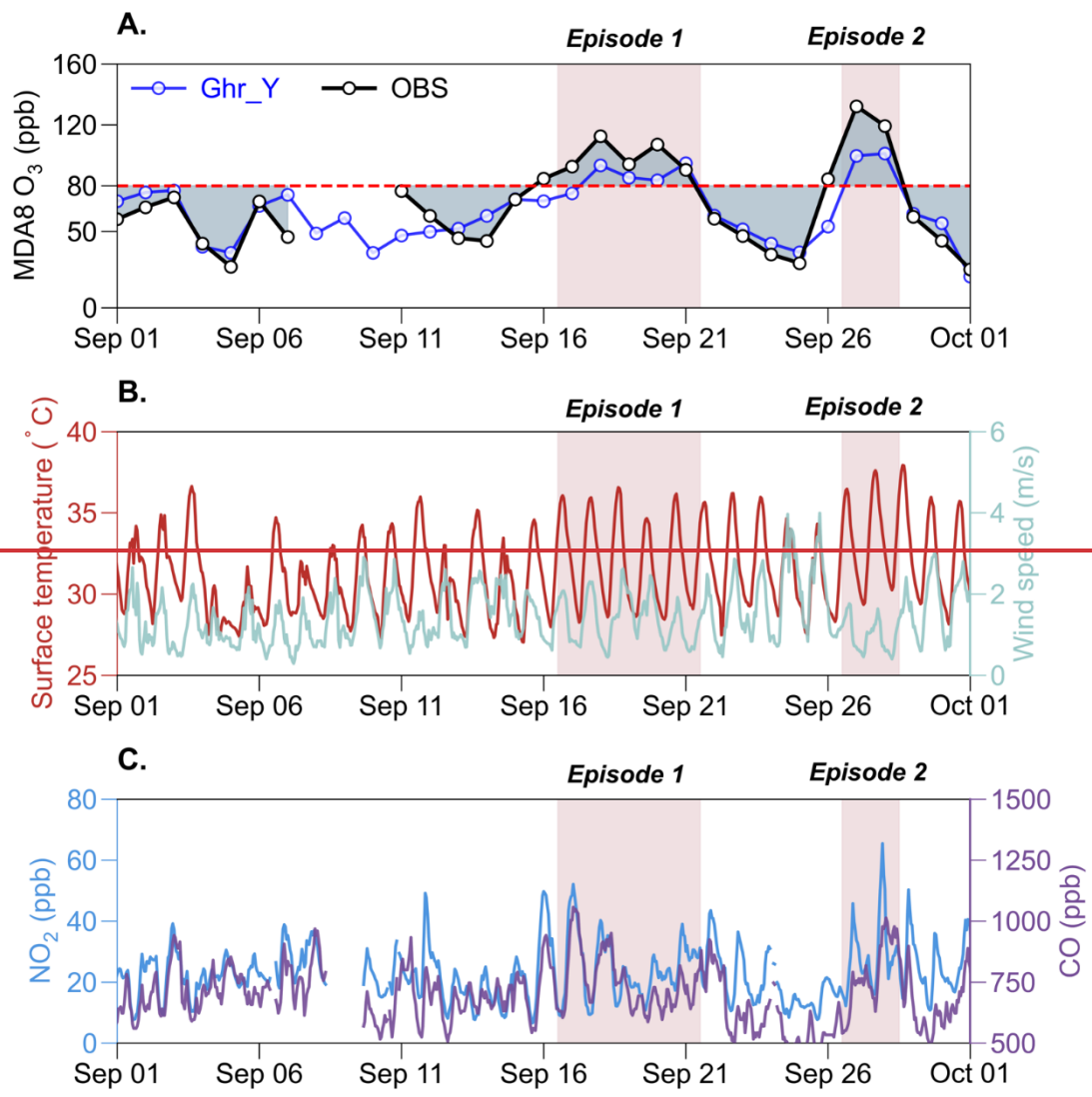
448 VOC levels can be highly sensitive in VOC-limited regions, where sufficient NO<sub>x</sub> concentrations mean that  
 449 even a small disturbance in VOCs can cause significant changes in O<sub>3</sub> concentrations. Similarly, metropolitan  
 450 areas, such as Guangzhou, often experience VOC-limited conditions or NO<sub>x</sub>-saturation (P. Wang et al., 2019).  
 451 Consequently, the UGS-BVOC case results in an overall increase in MDA8 O<sub>3</sub>. In contrast, the sole impact of  
 452 the UGS-LUCC effects (Figure 6B) is more extensive, influencing both the city center and suburban regions  
 453 and resulting in a general increase of approximately 1.1-2.0 ppb (+2.3-4.3%) in MDA8 O<sub>3</sub> levels, which can  
 454 be attributed to the higher temperature and solar radiation (Figure 5E-F). In Guangzhou, the transformation of  
 455 urban surfaces to natural vegetation due to UGS-LUCC results in lower albedo and consequently lower  
 456 temperatures. However, this change also reduces the height of the urban canopy, diminishing its shading  
 457 effects on solar radiation and paradoxically leading to higher temperatures in some regions. Therefore,  
 458 considering the UGS-LUCC effect, the decreased urban canopy height could lead to elevated temperatures,  
 459 thereby potentially increasing ozone production. However, the most significant results emerge under the  
 460 combined effect of UGS-BVOC and UGS-LUCC (Figure 6C), where a substantial increase in O<sub>3</sub>  
 461 concentration, ranging from 1.7-3.7 ppb (+3.8-8.5%), is observed across both the city center and suburban  
 462 regions. The observed increase suggests a potentially significant influence of UGS-BVOC emissions and  
 463 UGS-LUCC on ozone levels, indicating that these factors may play an important role in ozone pollution  
 464 research and should be carefully considered. This finding underscores the essential role that integrated urban  
 465 planning and environmental management play in controlling ozone pollution within metropolitan regions. By  
 466 considering UGS-BVOC emissions in air quality models and management plans, managers can make more  
 467 informed decisions to mitigate ozone levels and improve regional air quality.

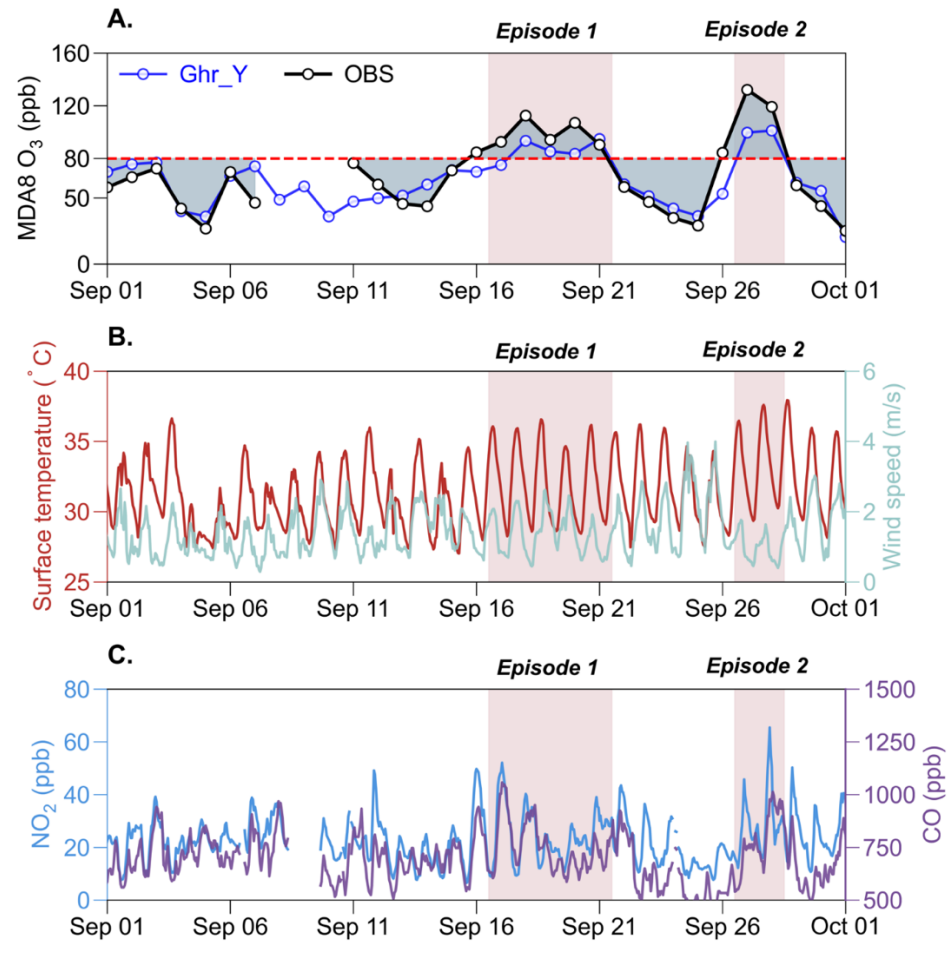


468  
 469 **Figure 6** The map of UGS-BVOC effects (a), LUCC effects (b), and combined effects (c) in MDA8 O<sub>3</sub>. Each map shows the difference in

470 average MDA8 O<sub>3</sub> concentrations for each case (Gdef\_Y, Ghr\_N, and Ghr\_Y) relative to the Gdef\_N case during September 2017.  
471

472 Previous studies have established that O<sub>3</sub> episodes are often accompanied by high temperatures and intense  
473 solar radiation, conditions that can exacerbate the UGS-BVOC emissions, critically affecting air quality model  
474 performance (Shan et al., 2023; Soleimanian et al., 2023). In this study, an O<sub>3</sub> episode is defined as a period  
475 of two or more consecutive days with MDA8 O<sub>3</sub> concentrations exceeding 160 µg/m<sup>3</sup> (~80 ppb) (Wu et al.,  
476 2020). Our analysis, as depicted in Figure 7A, identified two such episodes in Guangzhou City during  
477 September: the first from September 16 to 21 and the second from September 26 to 28. The Gdef\_N case  
478 successfully captures these episodes but tends to underestimate both MDA8 O<sub>3</sub> during these episodes. Figure  
479 7B-C highlight a notable reduction in wind speed during both episodes, particularly during the second episode.  
480 Despite some diffusion enhancement due to increased PBLH with rising surface temperatures (Figure S5S6),  
481 the surface temperature hike concurrently fosters O<sub>3</sub> production. Consequently, the episodes were dominated  
482 by a combination of temperature increases, which elevated O<sub>3</sub> concentrations, and wind speed decreases.  
483 Furthermore, Figure 7C illustrates that there was a significant spike in carbon monoxide (CO) concentrations  
484 during these episodes. CO, often used as a tracer in studies, indicates the worsening of diffusion conditions,  
485 leading to the accumulation of NO<sub>2</sub> - a primary O<sub>3</sub> precursor - thereby culminating in O<sub>3</sub> episodes in  
486 Guangzhou city.



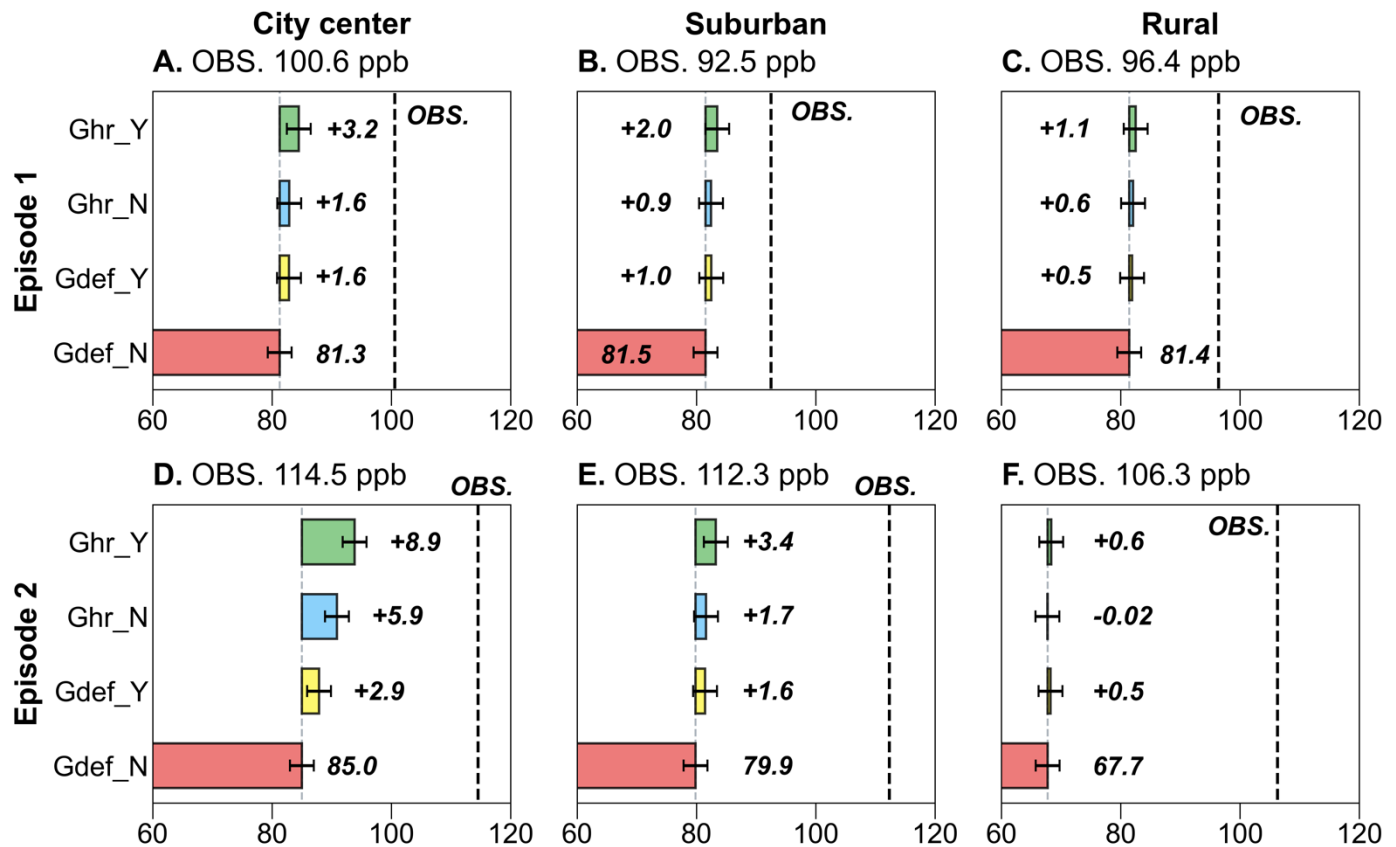


488  
489 **Figure 7** The comparison during September 2017 between the average values from simulation results grids which have air quality  
490 stations produced by the Gdef\_N case and the average observation values for MDA8 O<sub>3</sub> (A). (B) are the meteorological fields from the  
491 average values from the simulation result grids, which have the same locations as the air quality stations. (C) are the observed average  
492 values for NO<sub>2</sub> and CO concentrations from all air quality stations.

493 Figure 8 presents that in assessing the simulation of O<sub>3</sub> episodes, the Gdef\_N case, which initially  
494 underestimated O<sub>3</sub> concentrations, prompted an evaluation of improvements using different cases: UGS-  
495 LUCC (Ghr\_N), UGS-BVOC emissions (Gdef\_Y), and a combination of both (Ghr\_Y). The analysis,  
496 focusing on the city-center, suburban, and rural stations, reveals that all cases tend to underestimate O<sub>3</sub> levels  
497 between both episodes. However, incorporating the UGS-BVOC emissions into the model results in a notable  
498 increase in mean simulated MDA8 O<sub>3</sub> concentrations, particularly in the city center and suburban regions. For  
499 the sites in the city center region, the mean simulated MDA8 O<sub>3</sub> increased by +1.6 and +2.9 ppb (+1.8% and  
500 +3.3%, respectively), while for suburban sites, the increase was +1.0 ppb (+1.1%) and +1.6 ppb (+1.9%), with  
501 rural sites experiencing a smaller increase of only +0.5 ppb (+0.5%) and +0.5 ppb (+0.7%). This trend  
502 indicates a more pronounced impact in the city center and suburban regions compared to the rural region.  
503 Notably, the influence of the UGS-BVOC emissions on MDA8 O<sub>3</sub> in Episode 2 (+2.9 ppb) was significantly

505 greater than in Episode 1 (+1.6 ppb), suggesting that meteorological conditions in Episode 2 were more  
 506 conducive to the UGS-BVOC emissions, particularly in the city center region, which usually is VOC-limited  
 507 areas.

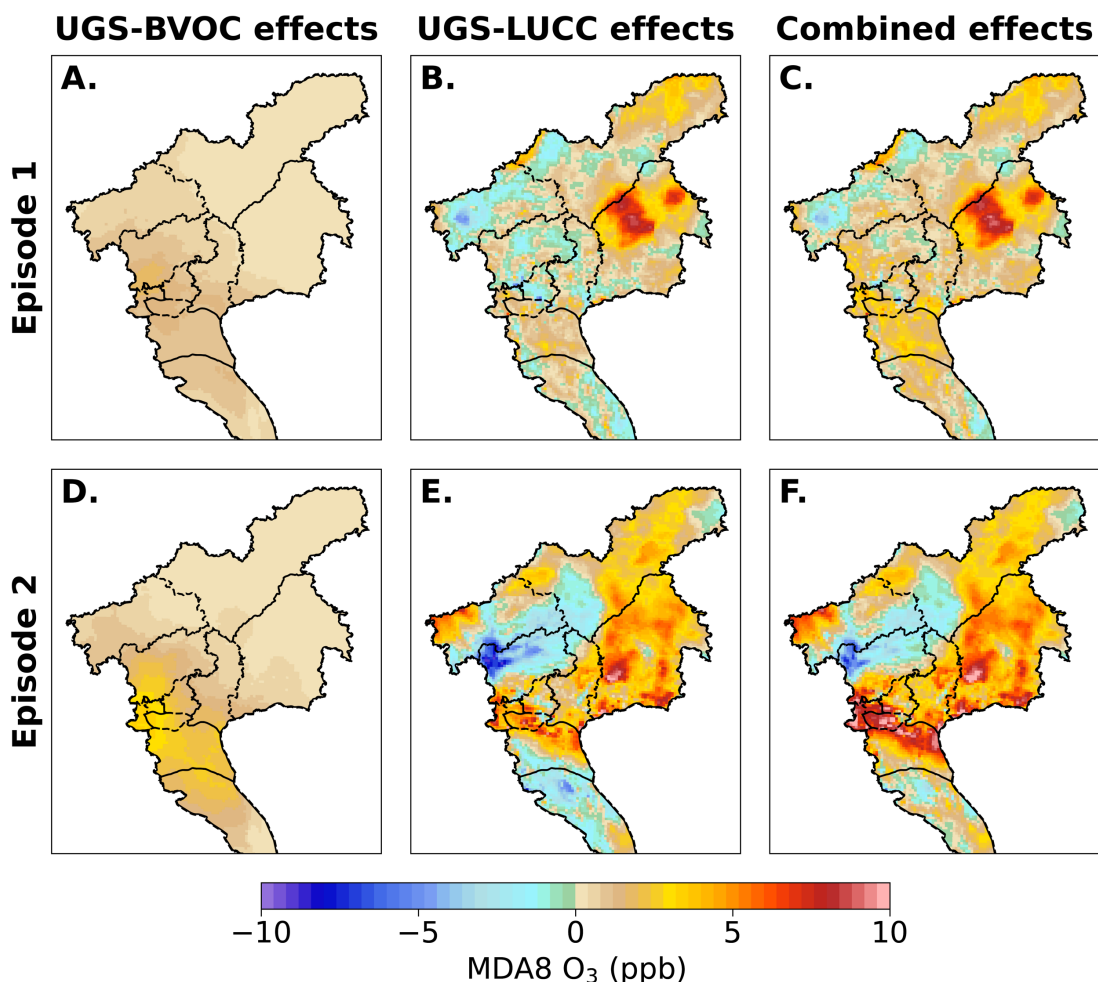
508  
 509 In Episode 1, the UGS-LUCC effects on  $O_3$  concentrations were comparable to that of UGS-BVOC emissions,  
 510 but in Episode 2, the UGS-LUCC effects led to a near doubling of urban MDA8  $O_3$  increase by 5.9 ppb  
 511 (+6.48%) compared to the UGS-BVOC emissions. This indicates that the UGS-LUCC effects play a non-  
 512 negligible role in  $O_3$  pollution studies, and the response to such changes under different meteorological  
 513 conditions varies significantly. Furthermore, due to the limited proportion of UGS in suburban and rural areas,  
 514 the increased effect of UGS on  $O_3$  is less pronounced in these regions, and nearly negligible in Episode 2.  
 515 While the UGS-BVOC emissions alone have a modest effect on  $O_3$  concentrations, their impact can become  
 516 significant when combined with the UGS-LUCC effects. For instance, the combined effects in the city center  
 517 region increased by 3.2 ppb (+3.7%) and 8.9 ppb (+10.0%) during Episode 1 and Episode 2, respectively.



518  
 519 **Figure 8** Comparison of simulated versus observed mean MDA8  $O_3$  concentrations across different cases for two episodes. The figure is  
 520 organized into columns representing city center (4 sites), suburban (3 sites), and rural (2 sites) settings (columns 1-3, respectively) and  
 521 rows indicating comparisons for episode 1 and episode 2 (rows 1 and 2, respectively).

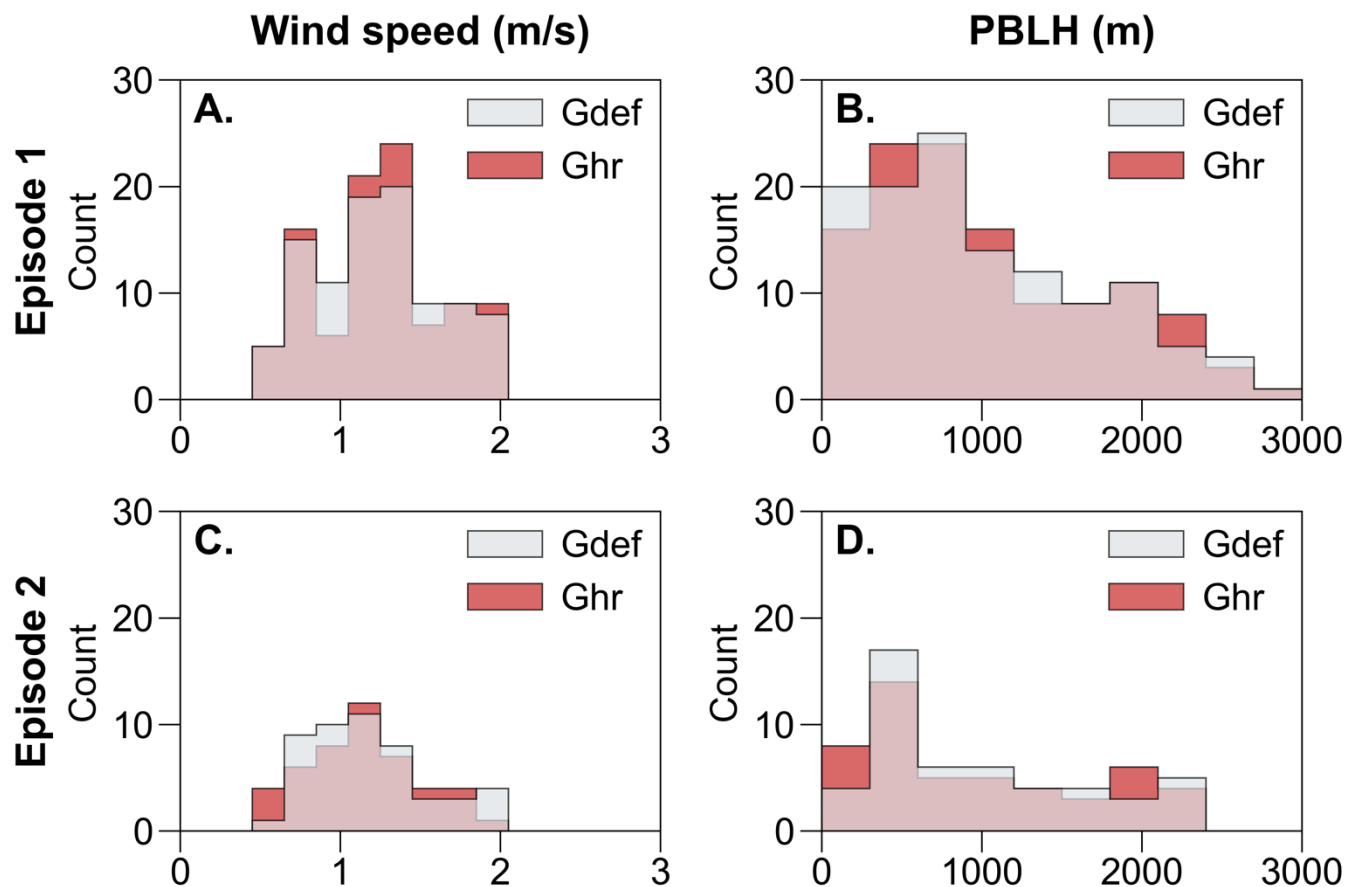
522 Figure 9 presents the map of each effect on MDA8  $O_3$  in both episodes and the influence of UGS-BVOC

524 emissions (Figure 9A and Figure 9D) on the MDA8 O<sub>3</sub> concentration during Episode 1 and Episode 2 ranges  
 525 from 0 to 2.0 ppb and 0 to 3.5 ppb, respectively, with the city center region witnessing the most significant  
 526 impact. This variance can be primarily ascribed to the heightened temperatures during Episode 2 (Figure 7B),  
 527 which create conditions more conducive to ozone generation through UGS-BVOC emissions. Furthermore,  
 528 the UGS-LUCC effect's maximal contribution to the urban MDA8 O<sub>3</sub> levels could escalate to 2.2 ppb in  
 529 Episode 1 and 23.7 ppb in Episode 2 while the combined effects of UGS-LUCC and UGS-BVOC emissions  
 530 are projected to enhance MDA8 O<sub>3</sub> concentrations to 4.8 ppb and 25.2 ppb for the respective episodes. This  
 531 marked increase in the episodes' contributions can be linked to the differential responsiveness of land use data  
 532 under various meteorological conditions. Notably, while the contribution from the UGS-BVOC effect during  
 533 Episode 2 substantially exceeds that of Episode 1, the incremental impact of UGS-LUCC on combined effects  
 534 in Episode 2 is notably smaller than in Episode 1. This phenomenon indicates that the escalated UGS-BVOC  
 535 emissions in Episode 2 may start to inhibit ozone production rates incrementally.



536  
 537 **Figure 9** The UGS-BVOC effects (A, D), the UGS-LUCC effects (B, E), and the combined effects (C, F) in Episode 1 and Episode 2,  
 538 respectively.  
 539

540 Figure 8 reveals that both observed O<sub>3</sub> episodes were primarily caused by reduced diffusion conditions.  
 541 Notably, the impact of the UGS-LUCC effects varied significantly between the two episodes. Analysis of  
 542 meteorological variables, specifically wind speed and PBLH, which are crucial for diffusion, demonstrate  
 543 distinct patterns. Figure 10 illustrates that during Episode 1, the UGS-LUCC effects led to a notable increase  
 544 in the frequency of higher wind speeds (1.2–1.4 m/s) and a simultaneous decrease in the frequency of lower  
 545 wind speeds (0.9–1.1 m/s). This shift in the wind speed distribution suggests an overall increase in average  
 546 wind speed due to the UGS-LUCC effects during Episode 1. In contrast, Episode 2 experiences a significant  
 547 decrease in wind speed frequency at 0.7–1.1 m/s, with an increase in the lower range of 0.5–0.7 m/s. This  
 548 suggests that the UGS-LUCC effects further reduce the already low wind speeds in Episode 2. Concerning  
 549 PBLH, the UGS-LUCC effects are observed to elevate PBLH during Episode 1, which led to a decrease in  
 550 PBLH during Episode 2. Therefore, the UGS-LUCC effects are markedly more pronounced in Episode 2 than  
 551 in Episode 1, contributing to a more substantial alteration of meteorological conditions affecting air dispersion  
 552 and, consequently, O<sub>3</sub> formation.



553  
 554 **Figure 10** The frequency of wind speed (column 1) and PBLH (column 2) in Episode 1 (row 1) and Episode 2 (row 2) driven by different  
 555 land use cover datasets.

556  
 557 **错误!未找到引用源。**Table 6 presents the overall results for the impacts of UGS-LUCC and UGS-BVOC on

558 MDA8 O<sub>3</sub> concentrations. The effects show slight variations across different regions during September, while  
 559 the effects during the two episodes exhibit more significant changes. In the city center region, which shows  
 560 the largest changes, the UGS-BVOC effect shows increases by +1.6 ppb in Episode 1 and +5.9 ppb in Episode  
 561 2, indicating that the UGS-BVOC effects influence MDA8 O<sub>3</sub> concentrations in the city center during ozone  
 562 episodes, while their impact is minimal in suburban and rural regions. These results highlight the important  
 563 effects of UGS-LUCC and UGS-BVOC in urban areas, especially during O<sub>3</sub> pollution periods.

564 **Table 6 Summary of Average MDA8 O<sub>3</sub> Concentrations (ppb) for Various Effects during September 2017.**

| Regions     | Periods   | UGS-BVOC effect | UGS-LUCC effect | Combined effect |
|-------------|-----------|-----------------|-----------------|-----------------|
| City center | Monthly   | +0.4            | 0.0             | 0.4             |
|             | Episode 1 | +1.6            | +1.6            | +3.2            |
|             | Episode 2 | +2.9            | +5.9            | +8.9            |
| Suburban    | Monthly   | +0.4            | 0.0             | 0.4             |
|             | Episode 1 | +1.5            | +0.9            | +2.0            |
|             | Episode 2 | +1.6            | +1.7            | +3.4            |
| Rural       | Monthly   | +0.4            | 0.0             | 0.4             |
|             | Episode 1 | +0.5            | +0.6            | +1.1            |
|             | Episode 2 | +0.5            | 0.0             | +0.5            |

## 565 4. Uncertainties and Limitations

566 In this study, we used land use and land cover data integrated at 1-km and 10-m resolutions to define the urban  
 567 boundary and characterize the spatial distribution of UGS in Guangzhou. Additionally, we incorporate high-  
 568 resolution LAI data, obtained through machine learning, as input for the MEGAN model. Using the WRF-  
 569 CMAQ model, we quantify the effects of UGS-BVOC, UGS-LUCC, and their combined impacts on ozone  
 570 concentrations in Guangzhou. However, some uncertainties and limitations remain.

571 First, the 10-m resolution land use and land cover data still cannot fully capture the spatial pattern of UGS in  
 572 Guangzhou. As shown in Figure S2, although UGS in Guangzhou is primarily composed of EBTs, most of  
 573 these EBTs are distributed along urban edges. This may result from distortions in the definition of urban extent,  
 574 such as misclassifying mixed urban-vegetation grids as urban grids, caused by the coarse resolution of the 1-  
 575 km land use and land cover data. The fuzzy definition of urban boundaries could lead to non-UGS areas being  
 576 misclassified as UGS, potentially resulting in an overestimation of UGS-BVOC emissions.

577  
 578 Second, due to resolution limitations, only larger patches of grassland, cropland, and woodland are recognized

581 as UGS, while smaller UGS vegetation, such as street trees, often goes undetected at a 10-m resolution. This  
582 omission can lead to an underestimation of the UGS-BVOC emissions.

583  
584 Third, the 10-m and 1-km resolution land use and land cover data, along with the growth forms and ecotype  
585 data, use simplified categorizations for grids, which cannot fully capture the diversity of vegetation species  
586 within UGS. Since different vegetation species have varying emission factors, this simplification introduces  
587 some errors. Similarly, the oversimplified classification of land grids limits this study's ability to provide  
588 specific planning strategies for UGS at the species level. Nevertheless, it can highlight the importance of  
589 considering UGS-BVOC and UGS-LUCC in air pollution prevention and control policies.

590  
591 Finally, Guangzhou, the study area, is a highly urbanized Chinese metropolis with a VOC-limited region  
592 (Gong et al., 2018; Liu et al., 2018; Zhou Kai et al., 2011). As a result, even a relatively small amount of VOC  
593 emissions, such as those from UGS-BVOC, can significantly impact ozone concentrations. Therefore,  
594 policymakers in Guangzhou should prioritize addressing the role of UGS-BVOC emissions in air pollution  
595 prevention and control. In other cities, particularly those with advanced urban development, high NO<sub>x</sub>  
596 emissions—often resulting from factors like high motor vehicle ownership—can lead to VOC-limited  
597 conditions. In such areas, it is equally important to emphasize the role of UGS-BVOC emissions in ozone  
598 pollution. In contrast, cities with lower NO<sub>x</sub> emissions identified as NO<sub>x</sub>-limited regions may experience  
599 minimal impact from UGS-BVOC emissions on ozone concentrations.

600  
601 **5. Conclusion**

602 The rapid urbanization process is accompanied by a higher frequency of ozone episodes. It has been  
603 increasingly recognized that UGS can potentially exacerbate ozone pollution under specific conditions due to  
604 the UGS-LUCC and UGS-BVOC emissions. Guangzhou, located in southern China and known as a pioneer  
605 city in reform and opening-up policies, has experienced rapid urbanization over the past thirty years, leading  
606 to increased challenges with ozone pollution. Despite efforts to reduce anthropogenic emissions, ozone  
607 episodes occur with relatively high frequency in Guangzhou. This study selected September 2017, a month  
608 with a high incidence of ozone episodes in Guangzhou, to estimate the UGS-BVOC emissions using the WRF-  
609 MEGAN model and quantitatively assess the impact of UGS-LUCC, UGS-BVOC, and their combined effects

610 on two ozone episodes in September 2017 using the CMAQ model. The major findings are shown as follows.

611

- 612 1. In September 2017, the UGS-BVOC emissions in Guangzhou totaled 666 Gg, with ISOP and TERP  
613 as the major species, emitting 213 and 136 Gg, respectively. Spatially, UGS-BVOC emissions were  
614 predominantly located in the city center region, attributed to the more extensive distribution of UGS  
615 there. The study also indicates that meteorological changes caused by UGS-LUCC do not significantly  
616 affect UGS-BVOC emissions. Instead, the formation of emission spatial distribution and intensity is  
617 closely related to local surface temperature and solar radiation. This understanding underscores the  
618 importance of considering local solar radiation and temperature conditions when assessing and  
619 modeling the distribution of the UGS-BVOC emissions, as they are pivotal in driving the spatial  
620 characteristics of these emissions.
- 621 2. Considering the UGS-BVOC and UGS-LUCC effects can effectively mitigate the underestimation of  
622 surface ozone concentrations by regional air quality models, though other factors such as inaccuracies  
623 in emissions inventories, chemical mechanisms, and meteorological inputs may also contribute to these  
624 underestimations. For instance, incorporating UGS-BVOC emissions results in an increase in ISOP  
625 concentration from 0.29 ppb to 0.35 ppb and from 0.23 ppb to 0.29 ppb under different land use cases  
626 (Gdef and Ghr), compared to a baselineobserved concentration of 0.3534 ppb. This significant  
627 enhancement in ISOP concentrations—the predominant component in BVOCs and the most crucial  
628 VOC for O<sub>3</sub> formation in the PRD—highlights two key points. Firstly, it indicates an improvement in  
629 the accuracy of BVOC concentration simulations. Secondly, this precise estimation of BVOCs and the  
630 consideration of UGS-LUCC has notably shifted the MB of MDA8 O<sub>3</sub> simulations from -3.6263 ppb  
631 to -0.75 ppb in the city center region. Additionally, the simulation of NO<sub>2</sub> concentrations also  
632 shows slight improvements, with the MB decreasing from 3.27 ppb to 2.81 ppb upon accounting for  
633 UGS-BVOCs and UGS-LUCC. Given that the UGS are often located in densely populated urban  
634 regions, their inclusion in air quality simulations is crucial for accurately modeling urban air quality.
- 635 3. The UGS-BVOC emissions have a remarkablesignificant impact on ozone concentrations, with  
636 increases ranging from 1.0-1.4 ppb (+2.3-3.2%) in the city center regions. However, when considering  
637 the combined UGS-LUCC and UGS-BVOC effects, the impact on MDA8 O<sub>3</sub> concentrations becomes  
638 remarkable, with values ranging from 1.7-3.7 ppb (+3.8-8.5%) in the city center region. This indicates  
639 the importance of considering both UGS-LUCC and UGS-BVOC impacts when discussing the  
640 influence of UGS on air quality. Since UGS exhibits different effects in various ozone episodes, it is

641 found that the impact of UGS on ozone levels is related to specific meteorological conditions. In the  
642 episodes of this study, the combined effects on MDA8 O<sub>3</sub> can reach up to 8.9 ppb in the city center  
643 region.

644

645 This study on ozone pollution in Guangzhou provides key insights for other cities on integrating UGS with  
646 air quality management. By including UGS-BVOC emissions and UGS-LUCC in the air quality model, the  
647 study demonstrates improved accuracy in predicting surface ozone concentrations, which can aid urban  
648 planners and environmental policymakers in refining their strategies to better address urban air pollution.  
649 Moreover, these findings encourage cities to integrate urban forestry into their land use planning and air quality  
650 frameworks, promoting environmental sustainability amid rapid urbanization.

## 651 **Data availability**

652 The WRF (Weather Research and Forecasting Model) code can be obtained from the official repository at  
653 <https://github.com/wrf-model/WRF>. The CMAQ (Community Multiscale Air Quality Model) code is  
654 accessible at <https://github.com/USEPA/CMAQ>. Model output data used for analysis and plotting, and the  
655 code used for simulations can be made available upon request (Haofan Wang, [wanghf58@mail2.sysu.edu.cn](mailto:wanghf58@mail2.sysu.edu.cn)).

## 656 **Author contributions**

657 HFW conceived the study, carried out the model simulations, and drafted the manuscript. YJL completed the  
658 data visualization. YML conceived and supervised this study, and reviewed and edited the paper. XL and YZ  
659 provided useful comments on the paper. QF supervised and funded the study. CS provided the meteorological  
660 data for model evaluation. SCL, YZ, TZ, and DLY provided the observation data for the evaluation of isoprene  
661 simulation.

## 662 **Competing interests**

663 The contact author has declared that neither they nor their co-authors have any competing interests.

664 **Acknowledgment**

665 The authors would like to thank the MEIC team from Tsinghua University for providing the anthropogenic  
666 emissions for this study. Meanwhile, we also thank Tianhe-2 for providing the computer resources.

667 **Financial support**

668 This work is jointly funded by the innovation Group Project of Southern Marine Science and Engineering  
669 Guangdong Laboratory (Zhuhai) (316323005), Guangdong Basic and Applied Basic Research Foundation  
670 (2020B0301030004, 2023A1515110103, 2023A1515010162), National Natural Science Foundation of China  
671 (42105097, 42075181, 42375182), Guangdong Science and Technology Planning Project (2019B121201002),  
672 and Science and Technology Planning Project of Guangzhou (2023A04J1544).

673 **Reference**

674 Allen, M.R., Ingram, W.J., 2002. Constraints on future changes in climate and the hydrologic cycle. *Nature*  
675 419, 224–232. <https://doi.org/10.1038/nature01092>

676 Arghavani, S., Malakooti, H., Bidokhti, A.A., 2019. Numerical evaluation of urban green space scenarios  
677 effects on gaseous air pollutants in Tehran Metropolis based on WRF-Chem model. *Atmos. Environ.* 214,  
678 116832. <https://doi.org/10.1016/j.atmosenv.2019.116832>

679 Burnett, R., Chen, H., Szyszkowicz, M., Fann, N., Hubbell, B., Pope, C.A., Apte, J.S., Brauer, M., Cohen, A.,  
680 Weichenthal, S., Coggins, J., Di, Q., Brunekreef, B., Frostad, J., Lim, S.S., Kan, H., Walker, K.D.,  
681 Thurston, G.D., Hayes, R.B., Lim, C.C., Turner, M.C., Jerrett, M., Krewski, D., Gapstur, S.M., Diver,  
682 W.R., Ostro, B., Goldberg, D., Crouse, D.L., Martin, R.V., Peters, P., Pinault, L., Tjepkema, M., van  
683 Donkelaar, A., Villeneuve, P.J., Miller, A.B., Yin, P., Zhou, M., Wang, L., Janssen, N.A.H., Marra, M.,  
684 Atkinson, R.W., Tsang, H., Quoc Thach, T., Cannon, J.B., Allen, R.T., Hart, J.E., Laden, F., Cesaroni,  
685 G., Forastiere, F., Weinmayr, G., Jaensch, A., Nagel, G., Concin, H., Spadaro, J.V., Burnett, R., Chen,  
686 H., Szyszkowicz, M., Fann, N., Hubbell, B., Pope, C.A., Apte, J.S., Brauer, M., Cohen, A., Weichenthal,  
687 S., Coggins, J., Di, Q., Brunekreef, B., Frostad, J., Lim, S.S., Kan, H., Walker, K.D., Thurston, G.D.,  
688 Hayes, R.B., Lim, C.C., Turner, M.C., Jerrett, M., Krewski, D., Gapstur, S.M., Diver, W.R., Ostro, B.,  
689 Goldberg, D., Crouse, D.L., Martin, R.V., Peters, P., Pinault, L., Tjepkema, M., van Donkelaar, A.,  
690 Villeneuve, P.J., Miller, A.B., Yin, P., Zhou, M., Wang, L., Janssen, N.A.H., Marra, M., Atkinson, R.W.,  
691 Tsang, H., Quoc Thach, T., Cannon, J.B., Allen, R.T., Hart, J.E., Laden, F., Cesaroni, G., Forastiere, F.,  
692 Weinmayr, G., Jaensch, A., Nagel, G., Concin, H., Spadaro, J.V., Burnett, R., Chen, H., Szyszkowicz,  
693 M., Fann, N., Hubbell, B., Pope, C.A., Apte, J.S., Brauer, M., Cohen, A., Weichenthal, S., Coggins, J.,  
694 Di, Q., Brunekreef, B., Frostad, J., Lim, S.S., Kan, H., Walker, K.D., Thurston, G.D., Hayes, R.B., Lim,  
695 C.C., Turner, M.C., Jerrett, M., Krewski, D., Gapstur, S.M., Diver, W.R., Ostro, B., Goldberg, D., Crouse,  
696 D.L., Martin, R.V., Peters, P., Pinault, L., Tjepkema, M., van Donkelaar, A., Villeneuve, P.J., Miller,

697 A.B., Yin, P., Zhou, M., Wang, L., Janssen, N.A.H., Marra, M., Atkinson, R.W., Tsang, H., Quoc Thach,  
698 T., Cannon, J.B., Allen, R.T., Hart, J.E., Laden, F., Cesaroni, G., Forastiere, F., Weinmayr, G., Jaensch,  
699 A., Nagel, G., Concin, H., Spadaro, J.V., 2018. Global estimates of mortality associated with long-term  
700 exposure to outdoor fine particulate matter. *Proc. Natl. Acad. Sci.* 115, 9592–9597.  
701 <https://doi.org/10.1073/pnas.1803222115>

702 Cao, J., Situ, S., Hao, Y., Xie, S., Li, L., 2022. Enhanced summertime ozone and SOA from biogenic volatile  
703 organic compound (BVOC) emissions due to vegetation biomass variability during 1981–2018 in China.  
704 *Atmospheric Chem. Phys.* 22, 2351–2364. <https://doi.org/10.5194/acp-22-2351-2022>

705 Chen, X., Wang, X., Wu, X., Guo, J., Zhou, Z., 2021. Influence of roadside vegetation barriers on air quality  
706 inside urban street canyons. *Urban For. Urban Green.* 63, 127219.  
707 <https://doi.org/10.1016/j.ufug.2021.127219>

708 Chowdhury, S., Pozzer, A., Haines, A., Klingmueller, K., Muenzel, T., Paasonen, P., Sharma, A.,  
709 Venkataraman, C., Lelieveld, J., 2022. Global health burden of ambient PM<sub>2.5</sub> and the contribution of  
710 anthropogenic black carbon and organic aerosols. *Environ. Int.* 159, 107020.

711 Cohen, A.J., Brauer, M., Burnett, R., Anderson, H.R., Frostad, J., Estep, K., Balakrishnan, K., Brunekreef, B.,  
712 Dandona, L., Dandona, R., Feigin, V., Freedman, G., Hubbell, B., Jobling, A., Kan, H., Knibbs, L., Liu,  
713 Y., Martin, R., Morawska, L., Pope, C.A., Shin, H., Straif, K., Shaddick, G., Thomas, M., van Dingenen,  
714 R., van Donkelaar, A., Vos, T., Murray, C.J.L., Forouzanfar, M.H., 2017. Estimates and 25-year trends  
715 of the global burden of disease attributable to ambient air pollution: an analysis of data from the Global  
716 Burden of Diseases Study 2015. *The Lancet* 389, 1907–1918. [https://doi.org/10.1016/S0140-6736\(17\)30505-6](https://doi.org/10.1016/S0140-6736(17)30505-6)

717 Dunlea, E.J., Herndon, S.C., Nelson, D.D., Volkamer, R.M., San Martini, F., Sheehy, P.M., Zahniser, M.S.,  
718 Shorter, J.H., Wormhoudt, J.C., Lamb, B.K., Allwine, E.J., Gaffney, J.S., Marley, N.A., Grutter, M.,  
719 Marquez, C., Blanco, S., Cardenas, B., Retama, A., Ramos Villegas, C.R., Kolb, C.E., Molina, L.T.,  
720 Molina, M.J., 2007. Evaluation of nitrogen dioxide chemiluminescence monitors in a polluted urban  
721 environment. *Atmospheric Chem. Phys.* 7, 2691–2704. <https://doi.org/10.5194/acp-7-2691-2007>

722 Emery, C., Liu, Z., Russell, A.G., Odman, M.T., Yarwood, G., Kumar, N., 2017. Recommendations on  
723 statistics and benchmarks to assess photochemical model performance. *J. Air Waste Manag. Assoc.* 67,  
724 582–598. <https://doi.org/10.1080/10962247.2016.1265027>

725 Friedl, M., Sulla-Menashe, D., 2019. MCD12Q1 MODIS/Terra+Aqua Land Cover Type Yearly L3 Global  
726 500m SIN Grid V006. <https://doi.org/10.5067/MODIS/MCD12Q1.006>

727 Fuhrer, J., Skärby, L., Ashmore, M.R., 1997. Critical levels for ozone effects on vegetation in Europe. *Environ.*  
728 *Pollut.* 97, 91–106. [https://doi.org/10.1016/S0269-7491\(97\)00067-5](https://doi.org/10.1016/S0269-7491(97)00067-5)

729 Gong, J., Hu, Z., Chen, W., Liu, Y., Wang, J., Liu, Z., Doherty, R.M., Wild, O., Hollaway, M., O'Connor,  
730 F.M., 2018. Urban expansion dynamics and modes in metropolitan Guangzhou, China. *Atmospheric*  
731 *Chem. Phys.* 72, 100–109. <https://doi.org/10.1016/j.landusepol.2017.12.025>

732 Guenther, A., Jiang, X., Shah, T., Huang, L., Kemball-Cook, S., Yarwood, G., 2020a. Model of Emissions of  
733 Gases and Aerosol from Nature Version 3 (MEGAN3) for Estimating Biogenic Emissions, in: Mensink,  
734 C., Gong, W., Hakami, A. (Eds.), *Air Pollution Modeling and Its Application XXVI*, Springer  
735 Proceedings in Complexity. Springer International Publishing, Cham, pp. 187–192.  
736 [https://doi.org/10.1007/978-3-030-22055-6\\_29](https://doi.org/10.1007/978-3-030-22055-6_29)

737 Guenther, A., Jiang, X., Shah, T., Huang, L., Kemball-Cook, S., Yarwood, G., 2020b. Model of Emissions of  
738 Gases and Aerosol from Nature Version 3 (MEGAN3) for Estimating Biogenic Emissions, in: Mensink,  
739 C., Gong, W., Hakami, A. (Eds.), *Air Pollution Modeling and Its Application XXVI*, Springer  
740 Proceedings in Complexity. Springer International Publishing, Cham, pp. 187–192.  
741 [https://doi.org/10.1007/978-3-030-22055-6\\_29](https://doi.org/10.1007/978-3-030-22055-6_29)

743 Guenther, A.B., Jiang, X., Heald, C.L., Sakulyanontvittaya, T., Duhl, T., Emmons, L.K., Wang, X., 2012a.  
744 The Model of Emissions of Gases and Aerosols from Nature version 2.1 (MEGAN2.1): an extended and  
745 updated framework for modeling biogenic emissions. *Geosci. Model Dev.* 5, 1471–1492.  
746 <https://doi.org/10.5194/gmd-5-1471-2012>

747 Guenther, A.B., Jiang, X., Heald, C.L., Sakulyanontvittaya, T., Duhl, T., Emmons, L.K., Wang, X., 2012b.  
748 The Model of Emissions of Gases and Aerosols from Nature version 2.1 (MEGAN2.1): an extended and  
749 updated framework for modeling biogenic emissions. *Geosci. Model Dev.* 5, 1471–1492.  
750 <https://doi.org/10.5194/gmd-5-1471-2012>

751 He, C.Q., Zou, Y., Lv, S.J., Flores, R.M., Yan, X.L., Deng, T., Deng, X.J., 2024. The importance of  
752 photochemical loss to source analysis and ozone formation potential: Implications from in-situ  
753 observations of volatile organic compounds (VOCs) in Guangzhou, China. *Atmos. Environ.* 320, 120320.  
754 <https://doi.org/10.1016/j.atmosenv.2023.120320>

755 Jin, S., Guo, J., Wheeler, S., Kan, L., Che, S., Fu, X., Liu, J., Ban-Weiss, G.A., Zhang, J., Huang, X., Ouyang,  
756 B., Popoola, O., Tao, S., Tiwari, A., Kumar, P., Xing, Y., Brimblecombe, P., 2017. Effects of canyon  
757 geometry on the distribution of traffic-related air pollution in a large urban area: Implications of a multi-  
758 canyon air pollution dispersion model. *Atmos. Environ.* 165, 111–121.  
759 <https://doi.org/10.1016/j.atmosenv.2017.06.031>

760 Jin, S., Guo, J., Wheeler, S., Kan, L., Che, S., Fu, X., Liu, J., Ban-Weiss, G.A., Zhang, J., Huang, X., Ouyang,  
761 B., Popoola, O., Tao, S., Tiwari, A., Kumar, P., Xing, Y., Brimblecombe, P., 2014. Evaluation of impacts  
762 of trees on PM2.5 dispersion in urban streets. *Atmos. Environ.* 99, 277–287.  
763 <https://doi.org/10.1016/j.atmosenv.2014.10.002>

764 Le Page, Y., Morton, D., Bond-Lamberty, B., Pereira, J.M.C., Hurt, G., 2015. HESFIRE: a global fire model  
765 to explore the role of anthropogenic and weather drivers. *Biogeosciences* 12, 887–903.  
766 <https://doi.org/10.5194/bg-12-887-2015>

767 Lelieveld, J., Klingmüller, K., Pozzer, A., Burnett, R.T., Haines, A., Ramanathan, V., 2019. Effects of fossil  
768 fuel and total anthropogenic emission removal on public health and climate. *Proc. Natl. Acad. Sci.* 116,  
769 7192–7197. <https://doi.org/10.1073/pnas.1819989116>

770 Lelieveld, J., Pozzer, A., Pöschl, U., Fnais, M., Haines, A., Münzel, T., 2020. Loss of life expectancy from air  
771 pollution compared to other risk factors: a worldwide perspective. *Cardiovasc. Res.* 116, 1910–1917.

772 Li, S., Lu, X., Wang, H., 2024. Anthropogenic emission controls reduce summertime ozone-temperature  
773 sensitivity in the United States. <https://doi.org/10.5194/egusphere-2024-1889>

774 Liu, Z., Doherty, R., Wild, O., Hollaway, M., O'Connor, F., 2018. Contrasting chemical environments in  
775 summertime for atmospheric ozone across major Chinese industrial regions: the effectiveness of emission  
776 control strategies. *Atmospheric Chem. Phys.* 21, 10689–10706. <https://doi.org/10.5194/acp-21-10689-2021>

777 Lohmann, U., Rotstayn, L., Storelvmo, T., Jones, A., Menon, S., Quaas, J., Ekman, A.M.L., Koch, D., Ruedy,  
778 R., 2010. Total aerosol effect: radiative forcing or radiative flux perturbation? *Atmospheric Chem. Phys.*  
779 10, 3235–3246. <https://doi.org/10.5194/acp-10-3235-2010>

780 Lombardozzi, D.L., Bonan, G.B., Smith, N.G., Dukes, J.S., Fisher, R.A., 2015. Temperature acclimation of  
781 photosynthesis and respiration: A key uncertainty in the carbon cycle-climate feedback. *Geophys. Res.*  
782 Lett. 42, 8624–8631. <https://doi.org/10.1002/2015GL065934>

783 Lu, X., Zhang, L., Wang, X., Gao, M., Li, K., Zhang, Yuzhong, Yue, X., Zhang, Yuanhang, 2020. Rapid  
784 Increases in Warm-Season Surface Ozone and Resulting Health Impact in China Since 2013. *Environ.*  
785 *Sci. Technol. Lett.* 7, 240–247. <https://doi.org/10.1021/acs.estlett.0c00171>

786 Luecken, D.J., Yarwood, G., Hutzell, W.T., 2019. Multipollutant modeling of ozone, reactive nitrogen and  
787 HAPs across the continental US with CMAQ-CB6. *Atmos. Environ.* 201, 62–72.

789 https://doi.org/10.1016/j.atmosenv.2018.11.060

790 Ma, H., Liang, S., 2022. Development of the GLASS 250-m leaf area index product (version 6) from MODIS  
791 data using the bidirectional LSTM deep learning model. *Remote Sens. Environ.* 273, 112985.  
792 https://doi.org/10.1016/j.rse.2022.112985

793 Ma, M., Gao, Y., Ding, A., Su, H., Liao, H., Wang, S., Wang, X., Zhao, B., Zhang, S., Fu, P., Guenther, A.B.,  
794 Wang, M., Li, S., Chu, B., Yao, X., Gao, H., 2022. Development and Assessment of a High-Resolution  
795 Biogenic Emission Inventory from Urban Green Spaces in China. *Environ. Sci. Technol.* 56, 175–184.  
796 https://doi.org/10.1021/acs.est.1c06170

797 Ma, M., Gao, Y., Wang, Y., Zhang, S., Leung, L.R., Liu, C., Wang, S., Zhao, B., Chang, X., Su, H., Zhang,  
798 T., Sheng, L., Yao, X., Gao, H., 2019. Substantial ozone enhancement over the North China Plain from  
799 increased biogenic emissions due to heat waves and land cover in summer 2017. *Atmospheric Chem.  
800 Phys.* 19, 12195–12207. https://doi.org/10.5194/acp-19-12195-2019

801 Masson-Delmotte, V., Zhai, P., Pirani, A., Connors, S.L., Péan, C., Berger, S., Caud, N., Chen, Y., Goldfarb,  
802 L., Gomis, M., others, 2021. Climate change 2021: the physical science basis. *Contrib. Work. Group  
803 Sixth Assess. Rep. Intergov. Panel Clim. Change* 2.

804 Meng, Y., Song, J., Zeng, L., Zhang, Y., Zhao, Y., Liu, X., Guo, H., Zhong, L., Ou, Y., Zhou, Y., Zhang, T.,  
805 Yue, D., Lai, S., 2022. Ambient volatile organic compounds at a receptor site in the Pearl River Delta  
806 region: Variations, source apportionment and effects on ozone formation. *J. Environ. Sci.* 111, 104–117.  
807 https://doi.org/10.1016/j.jes.2021.02.024

808 Myneni, R., Knyazikhin, Y., Park, T., 2015. MOD15A2H MODIS/Terra leaf area Index/FPAR 8-Day L4  
809 global 500m SIN grid V006. NASA EOSDIS Land Process. DAAC.

810 National Centers for Environmental Prediction, National Weather Service, NOAA, U.S. Department of  
811 Commerce, 2000. NCEP FNL Operational Model Global Tropospheric Analyses, continuing from July  
812 1999.

813 Pye, H.O.T., Murphy, B.N., Xu, L., Ng, N.L., Carlton, A.G., Guo, H., Weber, R., Vasilakos, P., Appel, K.W.,  
814 Budisulistiorini, S.H., Surratt, J.D., Nenes, A., Hu, W., Jimenez, J.L., Isaacman-VanWertz, G., Misztal,  
815 P.K., Goldstein, A.H., 2017. On the implications of aerosol liquid water and phase separation for organic  
816 aerosol mass. *Atmospheric Chem. Phys.* 17, 343–369. https://doi.org/10.5194/acp-17-343-2017

817 Qiu, J., Fang, C., Tian, N., Wang, H., Wang, J., 2023. Impacts of land use and land cover changes on local  
818 meteorology and PM2.5 concentrations in Changchun, Northeast China. *Atmospheric Res.* 289, 106759.  
819 https://doi.org/10.1016/j.atmosres.2023.106759

820 Ramanathan, V., Crutzen, P.J., Kiehl, J.T., Rosenfeld, D., Ramanathan, V., Crutzen, P.J., Kiehl, J.T.,  
821 Rosenfeld, D., Ramanathan, V., Crutzen, P.J., Kiehl, J.T., Rosenfeld, D., 2001. Aerosols, Climate, and  
822 the Hydrological Cycle. *Science* 294, 2119–2124. https://doi.org/10.1126/science.1064034

823 Salamanca, F., Martilli, A., Tewari, M., Chen, F., 2011. A Study of the Urban Boundary Layer Using Different  
824 Urban Parameterizations and High-Resolution Urban Canopy Parameters with WRF. *J. Appl. Meteorol.  
825 Climatol.* 50, 1107–1128. https://doi.org/10.1175/2010JAMC2538.1

826 Schlaerth, H.L., Silva, S.J., Li, Y., 2023. Characterizing Ozone Sensitivity to Urban Greening in Los Angeles  
827 Under Current Day and Future Anthropogenic Emissions Scenarios. *J. Geophys. Res. Atmospheres* 128,  
828 e2023JD039199. https://doi.org/10.1029/2023JD039199

829 Seinfeld, J.H., Pandis, S.N., Noone, K., 1998. *Atmospheric Chemistry and Physics: From Air Pollution to  
830 Climate Change*. *Phys. Today* 51, 88–90. https://doi.org/10.1063/1.882420

831 Shan, D., Du, Z., Zhang, T., Zhang, X., Cao, G., Liu, Z., Yao, Z., Tang, K., Liang, S., 2023. Variations, sources,  
832 and effects on ozone formation of VOCs during ozone episodes in 13 cities in China. *Front. Environ. Sci.*  
833 10, 1084592. https://doi.org/10.3389/fenvs.2022.1084592

834 Shindell, D., Kuylenstierna, J.C.I., Vignati, E., van Dingenen, R., Amann, M., Klimont, Z., Anenberg, S.C.,

835 Muller, N., Janssens-Maenhout, G., Raes, F., Schwartz, J., Faluvegi, G., Pozzoli, L., Kupiainen, K.,  
836 Höglund-Isaksson, L., Emberson, L., Streets, D., Ramanathan, V., Hicks, K., Oanh, N.T.K., Milly, G.,  
837 Williams, M., Demkine, V., Fowler, D., Shindell, D., Kuylenstierna, J.C.I., Vignati, E., van Dingen, R.,  
838 Amann, M., Klimont, Z., Anenberg, S.C., Muller, N., Janssens-Maenhout, G., Raes, F., Schwartz, J.,  
839 Faluvegi, G., Pozzoli, L., Kupiainen, K., Höglund-Isaksson, L., Emberson, L., Streets, D., Ramanathan,  
840 V., Hicks, K., Oanh, N.T.K., Milly, G., Williams, M., Demkine, V., Fowler, D., Shindell, D., Kuylenstierna,  
841 J.C.I., Vignati, E., van Dingen, R., Amann, M., Klimont, Z., Anenberg, S.C., Muller, N., Janssens-Maenhout,  
842 G., Raes, F., Schwartz, J., Faluvegi, G., Pozzoli, L., Kupiainen, K., Höglund-  
843 Isaksson, L., Emberson, L., Streets, D., Ramanathan, V., Hicks, K., Oanh, N.T.K., Milly, G., Williams,  
844 M., Demkine, V., Fowler, D., 2012. Simultaneously Mitigating Near-Term Climate Change and  
845 Improving Human Health and Food Security. *Science* 335, 183–189.  
846 <https://doi.org/10.1126/science.1210026>

847 Soleimanian, E., Wang, Y., Li, W., Liu, X., Griggs, T., Flynn, J., Walter, P.J., Estes, M.J., 2023. Understanding  
848 ozone episodes during the TRACER-AQ campaign in Houston, Texas: The role of transport and ozone  
849 production sensitivity to precursors. *Sci. Total Environ.* 900, 165881.  
850 <https://doi.org/10.1016/j.scitotenv.2023.165881>

851 Solomon, S., 2007. Climate change 2007—the physical science basis: Working group I contribution to the  
852 fourth assessment report of the IPCC. Cambridge university press.

853 Tiwari, A., Kumar, P., 2020. Integrated dispersion-deposition modelling for air pollutant reduction via green  
854 infrastructure at an urban scale. *Sci. Total Environ.* 723, 138078.  
855 <https://doi.org/10.1016/j.scitotenv.2020.138078>

856 Tomson, M., Kumar, P., Barwise, Y., Perez, P., Forehead, H., French, K., Morawska, L., Watts, J.F., 2021.  
857 Green infrastructure for air quality improvement in street canyons. *Environ. Int.* 146, 106288.  
858 <https://doi.org/10.1016/j.envint.2020.106288>

859 Wang, H., Liu, Z., Wu, K., Qiu, J., Zhang, Y., Ye, B., He, M., 2022. Impact of Urbanization on Meteorology  
860 and Air Quality in Chengdu, a Basin City of Southwestern China. *Front. Ecol. Evol.* 10, 845801.  
861 <https://doi.org/10.3389/fevo.2022.845801>

862 Wang, H., Liu, Z., Zhang, Y., Yu, Z., Chen, C., 2021. Impact of different urban canopy models on air quality  
863 simulation in Chengdu, southwestern China. *Atmos. Environ.* 267, 118775.  
864 <https://doi.org/10.1016/j.atmosenv.2021.118775>

865 Wang, N., Lyu, X., Deng, X., Huang, X., Jiang, F., Ding, A., 2019a. Role of vegetation in deposition and  
866 dispersion of air pollution in urban parks. *Atmos. Environ.* 201, 73–83.  
867 <https://doi.org/10.1016/j.atmosenv.2018.12.027>

868 Wang, N., Lyu, X., Deng, X., Huang, X., Jiang, F., Ding, A., 2019b. Aggravating O<sub>3</sub> pollution due to NO<sub>x</sub>  
869 emission control in eastern China. *Sci. Total Environ.* 677, 732–744.  
870 <https://doi.org/10.1016/j.scitotenv.2019.04.388>

871 Wang, P., Chen, Y., Hu, J., Zhang, H., Ying, Q., 2019. Attribution of Tropospheric Ozone to NO<sub>x</sub> and VOC  
872 Emissions: Considering Ozone Formation in the Transition Regime. *Environ. Sci. Technol.* 53, 1404–  
873 1412. <https://doi.org/10.1021/acs.est.8b05981>

874 WHO, 2021. WHO global air quality guidelines: particulate matter (PM<sub>2.5</sub> and PM<sub>10</sub>), ozone, nitrogen  
875 dioxide, sulfur dioxide and carbon monoxide. World Health Organization.

876 Wu, K., Yang, X., Chen, D., Gu, S., Lu, Y., Jiang, Q., Wang, K., Ou, Y., Qian, Y., Shao, P., Lu, S., 2020.  
877 Estimation of biogenic VOC emissions and their corresponding impact on ozone and secondary organic  
878 aerosol formation in China. *Atmospheric Res.* 231, 104656.  
879 <https://doi.org/10.1016/j.atmosres.2019.104656>

880 Yang, H., Chen, T., Lin, Y., Buccolieri, R., Mattsson, M., Zhang, M., Hang, J., Wang, Q., 2020. Integrated

881 impacts of tree planting and street aspect ratios on CO dispersion and personal exposure in full-scale  
882 street canyons. *Build. Environ.* 169, 106529. <https://doi.org/10.1016/j.buildenv.2019.106529>

883 Yao, Z., Huang, G., 2023. Effects of Land Use Changes Across Different Urbanization Periods on Summer  
884 Rainfall in the Pearl River Delta Core Area. *Int. J. Disaster Risk Sci.* 14, 458–474.  
885 <https://doi.org/10.1007/s13753-023-00497-8>

886 Yim, S.H.L., Wang, M., Gu, Y., Yang, Y., Dong, G., Li, Q., 2019. Effect of Urbanization on Ozone and  
887 Resultant Health Effects in the Pearl River Delta Region of China. *J. Geophys. Res. Atmospheres* 124,  
888 11568–11579. <https://doi.org/10.1029/2019JD030562>

889 Zhang, Y., Cao, F., 2015. Fine particulate matter (PM<sub>2.5</sub>) in China at a city level, *Sci. Rep.*, 5, 14884.

890 Zheng, J., Shao, M., Che, W., Zhang, L., Zhong, L., Zhang, Y., Streets, D., 2009. Speciated VOC Emission  
891 Inventory and Spatial Patterns of Ozone Formation Potential in the Pearl River Delta, China. *Environ.*  
892 *Sci. Technol.* 43, 8580–8586. <https://doi.org/10.1021/es901688e>

893 Zhou, D., Zhao, S., Zhang, L., Sun, G., Liu, Y., 2015. The footprint of urban heat island effect in China. *Sci.*  
894 *Rep.* 5, 11160.

895 Zhou Kai, Zhang Wen-jie, Wang Zhi-fang, Cao Wei, Peng Shao-lin, 2011. The influence of urbanization on  
896 atmospheric environmental quality in Guangzhou, China. 2011 Int. Conf. Electr. Technol. Civ. Eng.  
897 ICETCE 3667–3670. <https://doi.org/10.1109/ICETCE.2011.5776281>

898